A combined in silico/in vitro approach unveils common molecular requirements for efficient BVDV RdRp binding of linear aromatic N-polycyclic systems

Accepted Manuscript

A combined *in silico*/*in vitro* approach unveils common molecular requirements for efficient BVDV RdRp binding of linear aromatic N-polycyclic systems

A. Carta, I. Briguglio, S. Piras, P. Corona, R. Ibba, E. Laurini, M. Fermeglia, S. Pricl, N. Desideri, E.M. Atzori, P. La Colla, G. Collu, I. Delogu, R. Loddo

PII: S0223-5234(16)30255-0

DOI: 10.1016/j.ejmech.2016.03.080

Reference: EJMECH 8505

To appear in: *European Journal of Medicinal Chemistry*

Received Date: 20 January 2016

Revised Date: 16 March 2016

Accepted Date: 25 March 2016

Please cite this article as: A. Carta, I. Briguglio, S. Piras, P. Corona, R. Ibba, E. Laurini, M. Fermeglia, S. Pricl, N. Desideri, E.M. Atzori, P. La Colla, G. Collu, I. Delogu, R. Loddo, A combined *in silico*/*in vitro* approach unveils common molecular requirements for efficient BVDV RdRp binding of linear aromatic N-polycyclic systems, *European Journal of Medicinal Chemistry* (2016), doi: 10.1016/j.ejmech.2016.03.080.

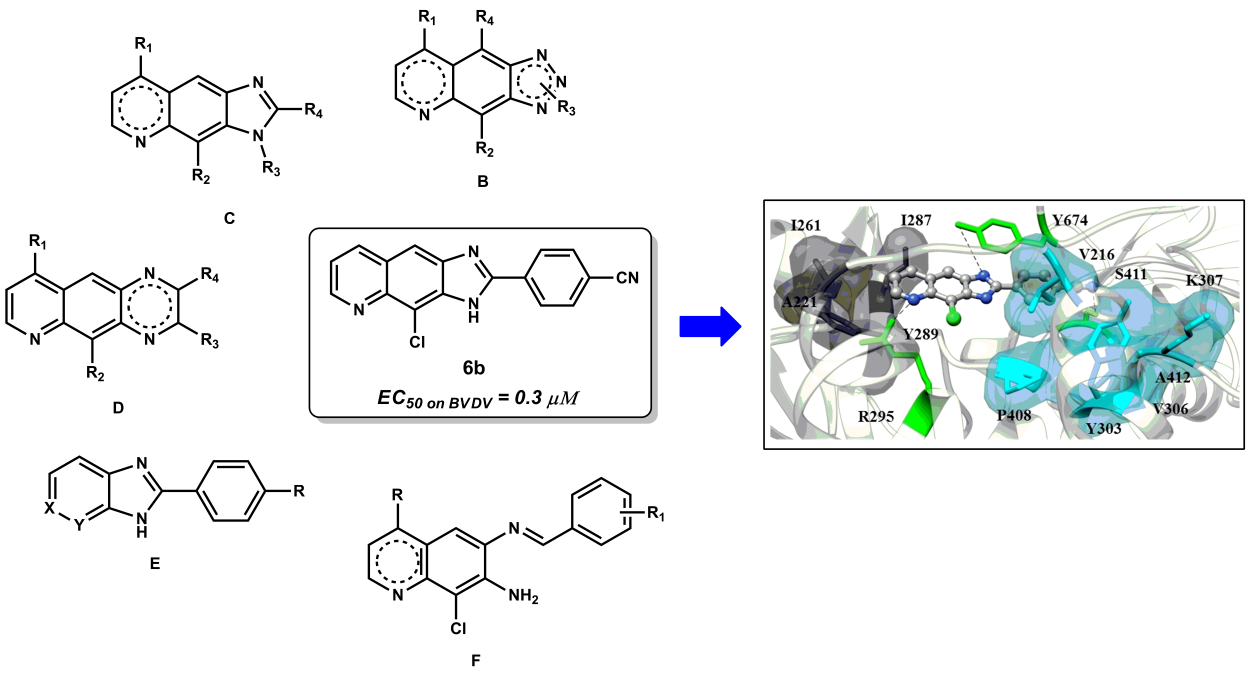

A combined *in silico*/*in vitro* approach unveils common molecular requirements for efficient BVDV RdRp binding of linear aromatic N-polycyclic systems.

A. Carta[†,■,*], *I. Briguglio*[†], *S. Piras*[†], *P. Corona*[†], *R. Ibba*[†], *E. Laurini*[§,■,#], *M. Fermeglia*[§,#], *S. Pricl*[§,#,*], *N. Desideri*[♦], *E. M. Atzori*[♦], *P. La Colla*[○], *G. Collu*[○], *I. Delogu*[○], *R. Loddo*[○,■]

[†] Dipartimento di Chimica e Farmacia, Università degli Studi di Sassari, via Muroni 23A, 07100 Sassari (SS)

[§] Molecular Simulations Engineering (MOSE) Laboratory, DEA, University of Trieste, Piazzale Europa 1, 34127 Trieste, Italy

[#] National Interuniversity Consortium for Material Science and Technology (INSTM), Research Unit MOSE-DEA, University of Trieste, Piazzale Europa 1, 32127 Trieste, Italy

[♦] Dipartimento di Chimica e Tecnologie del Farmaco, Sapienza, Università di Roma, P.le Aldo Moro, 5, 00185 Roma, Italy

[○] Dipartimento di Scienze Biomediche, Sezione di Microbiologia e Virologia, Università Cagliari, Cittadella Universitaria, 09042 Monserrato, Italy

KEYWORDS: Bovine viral diarrhea virus (BVDV); RNA-dependent RNA polymerase (RdRp) inhibitors; Imidazo[4,5-*g*]quinoline, Pyrido[2,3-*g*]quinoxaline, Aromatic N-polycyclic systems

ABSTRACT: In this work, we present and discuss a comprehensive set of both newly and previously synthesized compounds belonging to 5 distinct molecular classes of linear aromatic N-polycyclic systems that efficiently inhibits bovine viral diarrhea virus (BVDV) infection. A coupled *in silico*/*in vitro* investigation was employed to formulate a molecular rationale explaining the notable affinity of all molecules to BVDV RNA dependent RNA polymerase (RdRp) NS5B. We initially developed a three-dimensional common-feature pharmacophore model according to which two hydrogen bond acceptors and one hydrophobic aromatic feature are shared by all molecular series in binding the viral polymerase. The pharmacophoric information was used to retrieve a putative binding site on the surface of the BVDV RdRp and to guide compound docking within the protein binding site. The affinity of all compounds towards the enzyme was scored via molecular dynamics-based simulations, showing high correlation with *in vitro* EC_{50} data. The determination of the interaction spectra of the protein residues involved in inhibitor binding highlighted amino acids R295 and Y674 as the two fundamental H-bond donors, while two hydrophobic cavities HC1 (residues A221, I261, I287, and Y289) and HC2 (residues V216, Y303, V306, K307, P408, and A412) fulfill the third pharmacophoric requirement. Three RdRp (K263, R295 and Y674) residues critical for drug binding were selected and mutagenized, both *in silico* and *in vitro*, into alanine, and the affinity of a set of selected compounds towards the mutant RdRp isoforms was determined accordingly. The agreement between predicted and experimental data confirmed the proposed common molecular rationale shared by molecules characterized by different chemical scaffolds in binding to the

BVDV RdRp, ultimately yielding compound **6b** (EC_{50} = 0.3 µM; IC_{50}= 0.48 µM) as a new, potent inhibitor of this *Pestivirus*.

Introduction

DNA and RNA viruses represent a major cause of disease in humans and animals. Some of them, notably the *Ebola* and, previously, the *H1N1* viruses expressed their ability to create a pandemic scenario across globe, highlighting our unpreparedness to face infections caused by neglected pathogens that can easily spread worldwide. In this panorama, our multiannual program of antiviral research has focused on the design and synthesis of a wide series of small molecules endowed with antiviral activity. Various lead compounds emerged during the years, mainly active against representative viruses of *Flaviviridae* family.

The *Flaviviridae* is a large family of related positive-strand RNA viruses ($ssRNA^+$) that consists of three genera: *Flavivirus*, *Pestivirus* and *Hepacivirus*. Several globally important human and animal pathogens[1] are comprised within this group. The family members are genetically diverse but share similarities in genome organization, mechanisms of gene expression, and replication strategies.[2]

The *Flavivirus* genus currently contains 73 viruses classified as 53 species [3] divided into four groups: the tick-borne *Flaviviruses*, the mosquito-borne *Flaviviruses*, the not-known-vector *Flaviviruses*, and the non-classified *Flaviviruses*. A number of the arthropod-borne *Flaviviruses* cause disease in humans. Particularly, *Dengue Fever* (DFV), *Yellow Fever* (YFV), *West Nile* (WN), and *Japanese Encephalitis* (JE) viruses cause acute febrile illness, encephalitis, and hemorrhagic fevers, against which effective vaccines or established drug treatments for related

disease prevention and cure are still lacking. Attenuated YFV-based vaccines represent a noteworthy exception in this setting, although, despite their effectiveness, they sometimes shows toxic side effects that can be fatal,[4] and their utilization is incomplete in many areas.[5]

The *Pestivirus* genus includes animal pathogens of major economic impact for the livestock industry, such as *Swine Fever* virus (SFV), *Border Disease* virus (BDV), and *Bovine Viral Diarrhea* virus (BVDV).[6]. Particularly, BVDV establish a persistent infection in cattle that remain viremic throughout life and often succumb to fatal mucosal disease.[7] Furthermore, BVDV shows the ability to cross the placenta of susceptible animals causing a variety of fetal infections.[8] In the United States alone, a recent study revealed that the cost of exposing calves to BVDV in the feed-yard was $67.49/head. The vast majority of this amount, $58.83, was due to the loss in performance, primarily decreased efficiency. The remainder ($8.66) reflected an increase in mortality. The bottom line of this report is that, while few in number, persistently infected calves can have an economically devastating effect in feedlot cattle.[9] BVDV represents the prototypical *Pestivirus* virus and therefore is the best-characterized member of this group. Because of the genome organization, translation, replication strategy, and protein functions of *Pestiviruses*, BVDV is more closely related to Human Hepatitis C (HCV) virus than any of the classical *Flaviviruses*. As such, it has been widely adopted as a surrogate model for anti-HCV drug design and development.[10, 11] Lastly, BVDV is easily cultured *in vitro*, where it undergoes a complete replication cycle, and molecular clones are available for genetic studies.

The *Hepacivirus* genus features only HCV, the major cause of human hepatitis, globally.[12] The most recent World Health Organization (WHO) report estimates that 130–150 million people globally have chronic hepatitis C infection.[13]

At the moment, patients with severe cases of *Flavivirus* infections are treated only by supportive care, which includes intravenous fluids, hospitalization, respiratory support, and prevention of secondary infections.[14] In fact, despite worldwide extensive research and public health concern associated with *Flavivirus* diseases, no specific/routine treatment is available today to combat any *Flavivirus* infections, the sole exception being constituted by new drugs (e.g., simeprevir and sofosbuvir) currently in clinical trials for hepatitis C.[15, 16] Consequently, there is an urgent need for new lead compounds that efficiently target distinct stages of the viral replication cycle in a virus-specific way.

In this context, and in the framework of a long-lasting antiviral research program, our group designed and synthesized a series of new angular and linear N-polycyclic systems against representative ssRNA+ viruses. Small molecules inhibitors of BVDV has been reported in the literature with various scaffolds [17].

We recently reported a bicyclic system such as (E)-2-(1-(2-(2,4-dimethoxyphenyl)-1H-benzo[d]imidazol-5-yl)ethylidene)hydrazine-1-carbothioamide (227G, Fig. 1) that inhibits, in cell-based assays, both BVDV and HCV replication in the low micromolar range (EC_{50} values of 0.80 and 1.11 μM, respectively) [18].

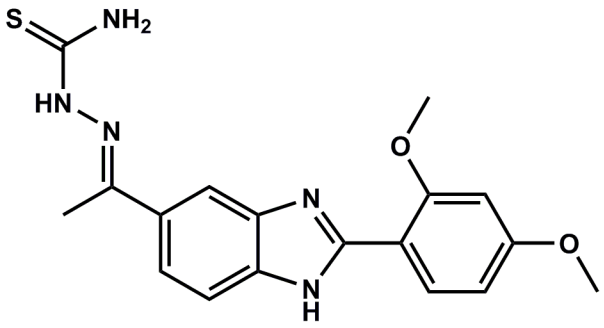

227G

$EC_{50\ on\ BVDV}$ = 0.80 μM

$EC_{50\ on\ HCV}$ = 1.11 μM

Fig. 1. Chemical structure and biological activity of benzimidazole derivative **227G**.

The molecular target was identified in the viral RNA dependent RNA polymerase (RdRp) [19] and dose−response curves indicate that 227G potently inhibits (IC_{50} =0.0020 ± 0.0004 μM) the BVDV RdRp activity [20]. In an attempt to widen the knowledge on the anti BVDV activity of nitrogen-containing heterocyclic compounds we complicate the bicyclic system and we synthesized a series of [4,7]phenantroline derivatives [21] (Fig. 2). At first, we demonstrated that some [4,7]phenantroline derivatives were fairly active against BVDV *in vitro*, compound **A1** being particularly promising against both BVDV and HCV (Fig. 2). Next, *in silico* experiments on the putative final target, the HCV RNA-dependent RNA-polymerase (RdRp) NS5B, contributed to develop a molecular-based rationale for the structure-activity relationship (SAR) for these compounds [21]. The target enzyme was identified in the light of some similarities between a number of our active compounds and the non-nucleoside inhibitor of HCV NS5B ((2s)-2-[(2,4-dichloro-benzoyl)-(3-trifluoromethyl-benzyl)-amino]-3-phenyl-propionic acid), hereafter named Shire A [22].

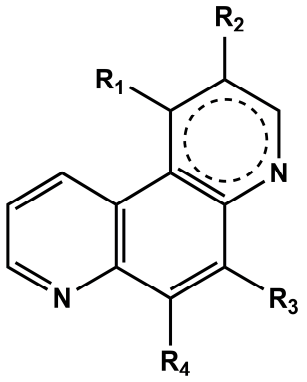

A

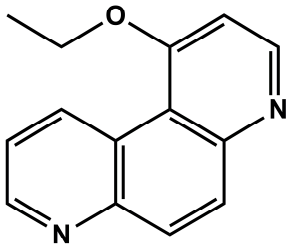

A1

$EC_{50\ on\ BVDV}$ = 6 μM

$IC_{50\ calculated\ on\ HCV\ NS5B}$ = 12 μM

Fig. 2. Chemical structures of [4,7]phenantroline derivatives **A**.[21]

Unfortunately, the most potent angular derivatives turned out to be non-selective inhibitors of BVDV. Compound A1, in fact, resulted active against non only BVDV but also against CVB-2 and Sb-1 (EC_{50} = 5 and 17 μM, respectively). With the aim of improving both their potency and selectivity towards BVDV, we next conceived and synthesized three new classes of linear aromatic N-tricyclic compounds derived from the expansion of the quinoline nucleus with 1,2,3-triazole, imidazole or pyrazine (Fig. 3).[23] Thus, triazolo[4,5-*g*]quinoline (**B**), imidazo[4,5-*g*]quinoline (**C**), and pyrido[2,3-*g*]quinoxaline derivatives (**D**) were tested in cell-based assays for both cytotoxicity and antiviral activity against representative members of several virus families, and found endowed with promising antiviral activity and selectivity index against several pathogenic RNA viruses.[23]

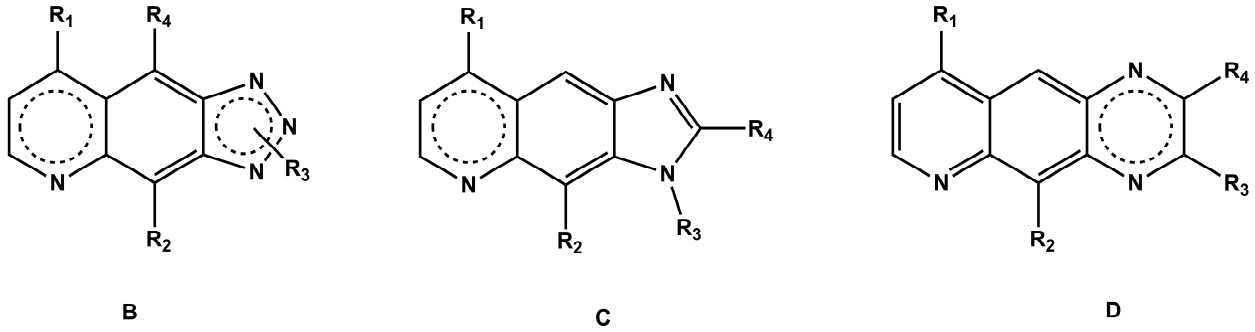

Fig. 3. Chemical structures of triazolo[4,5-*g*]quinoline (**B**), imidazo[4,5-*g*]quinoline (**C**), and pyrido[2,3-*g*]quinoxaline derivatives (**D**).

Interestingly, while selective anti-BVDV activity was reported for all three classes of compounds in Fig. 3, derivatives endowed with substantial anti-BVDV activity were more numerous among imidazoquinolines and pyridoquinoxalines than among triazoloquinolines. Nevertheless, each class contained at least one potent and selective molecule. On this basis, selected leads from these series were then evaluated for anti-HCV activity in a replicon system and tested in enzyme assays for activity against the RdRps of BVDV and HCV. 4-Chloro-2-(4-nitrophenyl)-3H-imidazo[4,5-g]quinoline (**C2**, Fig. 4) thus emerged as the most potent and selective compound against BVDV (EC_{50} = 1.2 μM, CC_{50}> 100 μM). [32] It also proved to be active, although only moderately selective, against HCV. These results suggested that, although with different efficiency, compound (**C2**) (Fig. 4) targets both viral RdRps. Consequently, to broad our knowledge concerning the SAR of imidazo[4,5-*g*]quinolines, the chemical structure of **C2** was simplified via the elimination of the central ring or the opening of the imidazole ring, leading to various imidazopyridines (**E**) and N-benzylidenequinolinamines (**F**), respectively (Fig. 4). Remarkably, just a few imidazopyridine derivatives resulted active against BVDV, while all N-benzylidenequinolinamines maintained their antiviral behavior. Particularly, compounds **F1**

and **F2** showed EC_{50} values of the same order of magnitude of the reference drug 2′-C-methyl-guanosine (1.1 μM) [24] - as shown in Fig. 4.

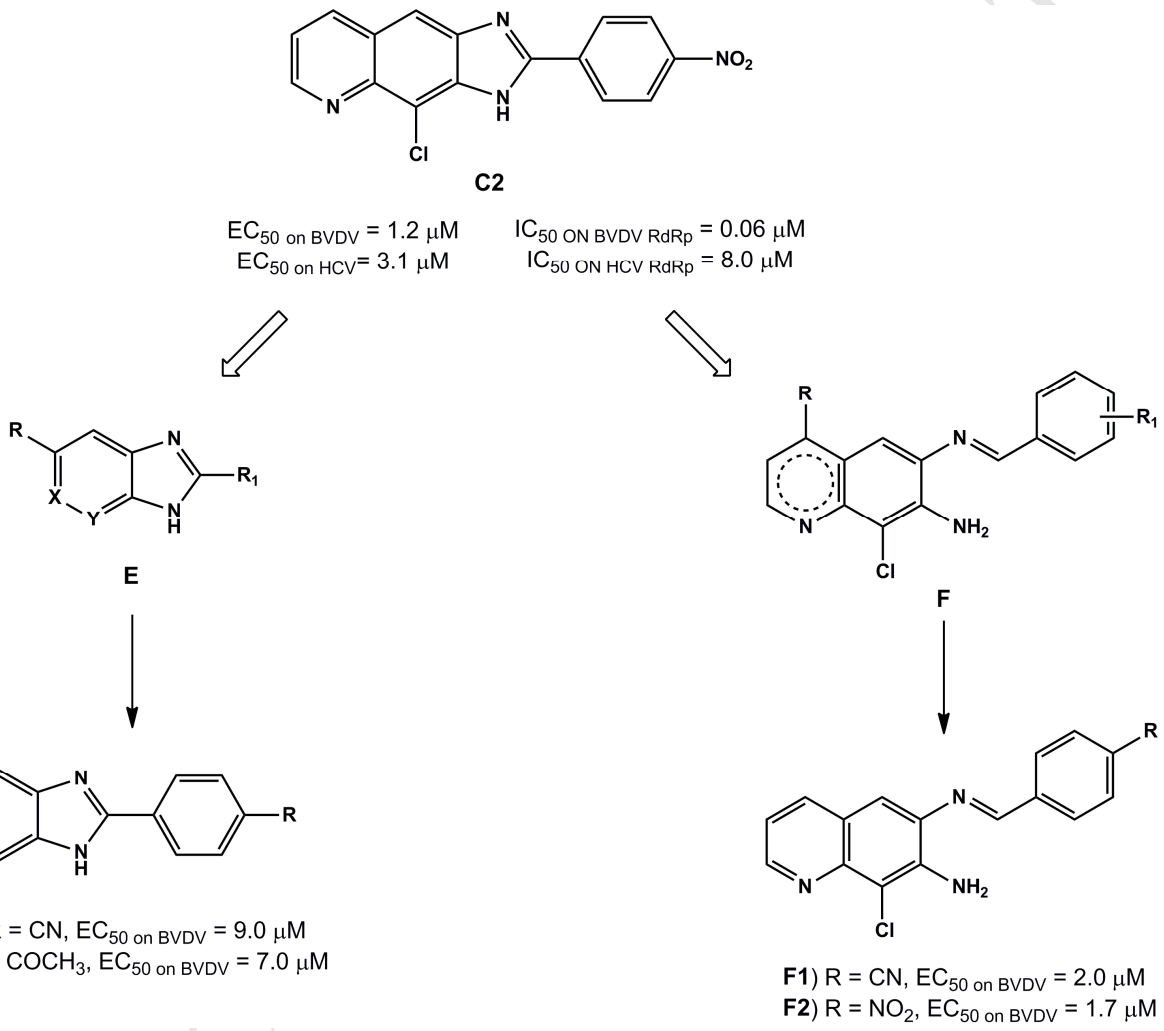

Fig. 4. Chemical structure of lead compound **C2** and the rationale leading to its subsequent modifications.

The selective anti-BVDV activity of pyridoquinoxaline-based compounds (**D**)[23] was also further investigated by synthesizing further derivatives, among which the thienyl derivative (**D1**)

showed selectivity, good potency and an interesting balance between activity and cytotoxicity (Fig. 5).

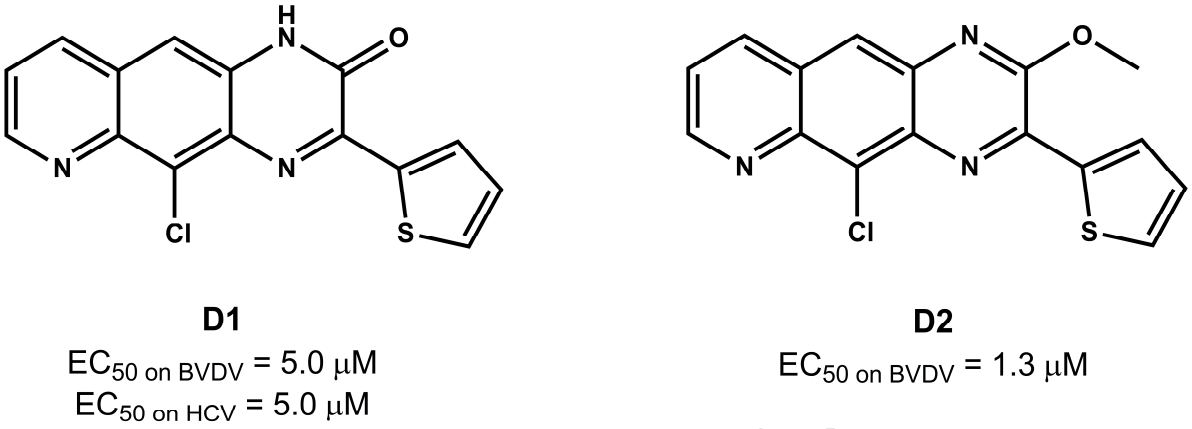

D1
$EC_{50\ on\ BVDV}$ = 5.0 μM
$EC_{50\ on\ HCV}$ = 5.0 μM

D2
$EC_{50\ on\ BVDV}$ = 1.3 μM

Fig. 5. Chemical structures of lead compounds **D1** and **D2**.

Furthermore, the derivatives bearing different substituents on the N atom at position 1 or the O atom at position 2 were tested in cell-based assays for cytotoxicity and antiviral activity. The 5-chloro-2-methoxy-3-(thiophen-2-yl)pyrido[2,3-g]quinoxaline **D2**, totally devoid of cytotoxicity, emerged for its selective and potent antiviral activity against BVDV (EC_{50}= 1.3 μM, Fig. 5). Molecular modeling studies confirmed the BVDV RdRp as the target enzyme for these compounds and allowed the identification of important molecular determinants for their NS5B inhibition.[25]

To expand the SAR investigation on the above linear N-tricyclic systems, in the present paper we initially designed and synthesized new imidazo[4,5-*g*]quinolines derived by further development of the basic compound 2-phenyl-3H-imidazo[4,5-g]quinoline (**C1**) (EC_{50} = 4 μM, CC_{50} > 100 μM).[32] To this purpose, we modulated substituents at positions R_1, R_2, and/or R_3, or replaced

the phenyl ring with a heterocyclic moiety, as illustrated in Fig. 6. Specifically, substituents were chosen with the aim of evaluating the influence of electron donating groups (EDGs) or electron withdrawing groups (EWGs) on the phenyl group (R_3 in Fig. 6), of the Cl atom at position R_1, and/or general steric hindrance of substituents in R_2 on the antiviral activity of the resulting molecules.

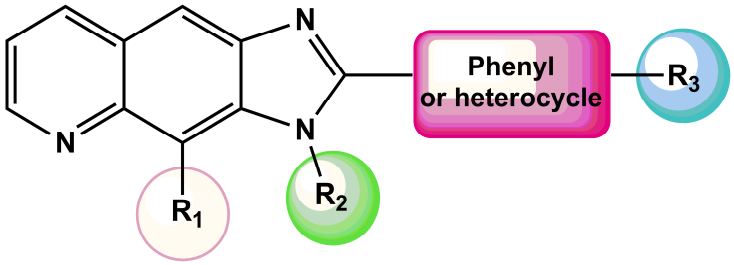

Fig. 6. Proposed rational modifications of lead compound **C1** (R_1 = Cl, R_2 = H, R_3 = H; EC_{50} = 4.0 μM, CC_{50}>100μM).

Thus, we synthesized compounds bearing either chlorine or hydrogen at position R_1 to quantify the specific contribution of the halogen to the compound affinity for the binding site of the BVDV NS5B. In addition, a large moiety such as methyl cyclohexyl was inserted in R_2 to test the tolerance of the viral polymerase binding pocket towards substituent bulkiness. In combination with the two modifications mentioned above, EDGs or EWGs were inserted at the 4′ position or at the 2’ and 4’ positions of the phenyl ring (R_3 in Fig. 6). Lastly, we synthesized and assayed a furan(3)-yl derivative since no compound bearing a heterocyclic moiety at position 2 was previously reported. All modifications are indicated in details in Scheme 1.

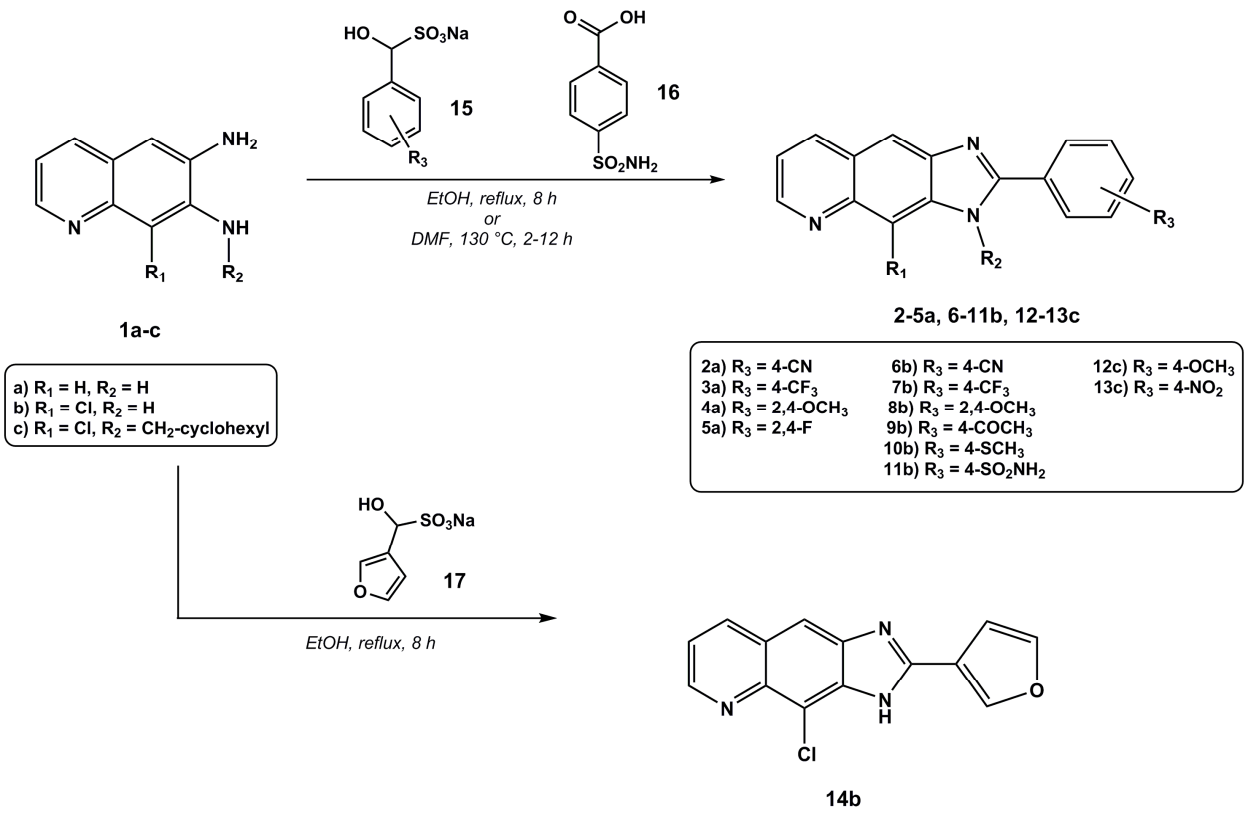

Scheme 1. Selected chemical modifications of lead compound **C1** and synthetic pathways leading to the compounds **2-5a**, **6-11b**, **12-13c**, and **14b**.

In the light of the encouraging results obtained, we next proceeded by performing a parallel *in silico/in vitro* analysis of the best compounds of all previous (**B**-**F**)[23, 24] and present series and determined the common molecular determinants leading to their successful BVDV RdRp inhibition.

Chemistry

The synthetic route to obtain the designed 3*H*-imidazo[4,5-*g*]quinoline derivatives (**2-5a**, **6-11b**, **12-13c**, and **14b**) is shown in Scheme 1. The diamines **1a-c** react with appropriate bisulphite compounds (**15** and **17**) in refluxed ethanol or in dimethylformammide (DMF) at 130 °C for 2-12

h, to give the corresponding 3*H*-imidazo[4,5-*g*]quinolines (**2-5a**, **6-10b**, **12-13c**, and **14b**) in good yield (54-90%), with the exception of **13c** (25%). Compound 4-(4-chloro-3*H*-imidazo[4,5-*g*]quinolin-2-yl)benzenesulfonamide (**11b**) was in turn prepared by condensation of the diaminoquinoline **1b** with 4-sulfamoylbenzoic (**16**) and polyphosphoric acid for 4 h at 200 °C (25% yield). 6,7-Diaminoquinolines **1a-c** intermediates were prepared following the procedure previously described.[23, 26] Bisulphite compounds (**15** and **17**), were obtained by reacting the aldehydes with $Na_2S_2O_5$ in hydroalcoholic solution.[23] Aldehydes and inorganic reagents were commercially available.

Results and discussion

As discussed above, the original hypothesis motivating the current work proposed that specific substituents at different positions of the scaffold of the lead compound **C1** (Fig. 6) would be selective and effective inhibitors of the BVDV RdRp. To investigate this proposition, compounds **2-5a**, **6-11b**, **12-13c**, and **14b** were synthesized and evaluated for activity and selectivity against BVDV and other ssRNA+, ssRNA-, dsRNA and DNA viruses.. Data from these experiments are presented in Tables 1 and S1, respectively.

Table 1. Cytotoxicity and antiviral activity of 3H-imidazo[4,5-g]quinoline derivatives (**2-5a**, **6-11b**, **12-13c**, and **14b**) against BVDV. Data represent mean values of three independent determinations. Variation among duplicate samples was less than 15%.

Compound	MDBK[a] CC_{50} (μM)	BVDV[b] EC_{50}(μM)	S.I.	Compound	MDBK[a] CC_{50} (μM)	BVDV[b] EC_{50}(μM)	S.I.
2a	>100	4.0	>25.0	**10b**	>100	6.1	>16.4
3a	>100	7.0	>14.2	**11b**	>100	>100	-
4a	>100	3.4	>29.4	**12c**	20	5.0	4.0
5a	>100	6.0	>16.7	**13c**	33	5.0	>6.6

6b	>100	**0.3**	>333.3	**14b**	>100	2.0	>50.0
7b	>100	2.0	>50.0	**2'-MeGua**	>10	1.1	>9.1
8b	>100	6.3	>15.9	**Ribavirine**	5.0	1.3	3.8
9b	>100	5.8	>17.2				

[a] Compound concentration (μM) required to reduce the viability of mock-infected MDBK cells by 50%, as determined by the MTT method.
[b] Compound concentration (μM) required to achieve 50% protection of MDBK cells from BVDV-induced cytopathogenicity, as determined by the MTT method.
2'-MeGua = 2'-C-methyl-guanosine.

From the results shown in Table 1 it is apparent that all compounds, with the singular exception of **11b**, were significantly active, with EC_{50} ranging between 0.3 and 7 μM along with low cytotoxicity (CC_{50} > 100 μM, except for compounds **12c** and **13c**, for which CC_{50} = 20 and 33 μM, respectively). The selectivity index (S.I.), which is a parameter of preferential antiviral activity of a compound in relation to its cytotoxicity (CC_{50}/EC_{50}), of all new compounds is also tabulated in Table 1. As can be seen, the SI index values of the title compounds were substantially better than those of the positive controls, 2'-C-methyl-guanosine (S.I. = 9.1) and of the gold-standard reference ribavirin, for which S.I. = 3.8.

Preliminary SARs shows that the presence of a chlorine substituent on the scaffold of compound **C1** (R_1 in Fig. 6) is slightly more beneficial to the antiviral activity of the relevant compounds (e.g. **6b**, EC_{50} = 0.3 μM; **7b**, EC_{50} = 2.0 μM; **8b**, EC_{50} = 6.3 μM) with respect to those featuring an hydrogen atom at the same position (**2a**, EC_{50} = 4.0 μM; **3a**, EC_{50} = 7.0 μM; **4a**, EC_{50} = 3.4 μM). Within the same molecular series, the presence of either EWGs [e.g., -CN (**2a** and **6b**, EC_{50} = 4.0 μM and 0.3 μM, respectively), $–CF_3$ (**3a** and **7b**, EC_{50} = 7.0 μM and 2.0 μM, respectively), $–COCH_3$ (**9b**, EC_{50} = 5.8 μM), –F (**5a**, EC_{50} = 6.0 μM) and $–NO_2$ (**14c**, EC_{50} = 5.0 μM)] or EDGs [e.g., 2,4-OCH_3 (**4a** and **8b**, EC_{50} = 3.4 μM and 6.3 μM, respectively), and -

SCH_3 (**10b**, EC_{50} = 6.1 μM)] retains the antiviral activity with respect to the lead compounds **C1** (EC_{50} = 4 μM). Finally, although some new compounds showed a modest and scattered activity against other than BVDV viruses (Table S1), we can reasonable identify these new quinolone derivatives as selective and potent anti-BVDV agents.

The occurrence of a bulky substituent in R_2 does not result in an appreciable effect on the activity of the relevant compound **13c** with respect to the analogous, unsubstituted molecule **C2** (EC_{50} = 5.0 μ and 1.2 μM, respectively), implying that the target BVDV RdRp can accommodate a large group at that position with minimum steric hindrance. At the same time, however, while compound **C2** was devoid of cytotoxicity (CC_{50} > 100 μM), the presence of the cycloaliphatic moiety on **13c** seems to endow this compound with some toxic effects (CC_{50} = 33 μM). An analogous behavior can be observed in the case of compound **12c**.

Finally, compound **14b**, featuring the replacement of the phenyl ring on the scaffold of **C1** with a heterocyclic moiety (i.e., furane), showed better antiviral activity (EC_{50} = 2.0 μM) than the C1 derivative, preserving at the same time its non-toxic character (CC_{50}> 100 μM).
Globally, the combination between an electron withdrawing group such as –CN on phenyl position 4' and a chlorine substituent on position 4 of the imidazo[4,5-*g*] quinoline scaffold led to define compound **6b** as new lead compound, bearing EC_{50} = 0.3 μM, no cytotoxicity and a S.I. > 333.3.

Ordinarily, the development of a pharmacophore model aims at creating a powerful tool for the design of new and possibly more potent molecules with respect to a specific target. In this work, however, the common feature pharmacophore approach was exploited to identify the molecular requirements shared by all series of compounds (i.e., previously synthesized **B**-**F** series [23, 24], and newly synthesized compounds **2-5a**, **6-11b**, **12-13c**, and **14b**) in determining their inhibitory

activity against the BVDV RdRp. Accordingly, a selection of 31 compounds among the entire sets were selected, along with their experimentally BVDV EC_{50} values, as the training set for the development of the corresponding three-dimensional (3D) pharmacophore model (Fig. S1).

The calculated best-fit values ranked Hypo1, which consists of two Hydrogen Bond Acceptor features (HBA) and one Hydrophobic Aromatic feature (HY_AR) (Fig. 7A), as the best model. Accordingly, the most active compounds of training set belonging to the 4 different scaffolds considered in this paper were mapped onto Hypo1, as shown in Fig.7B-F.

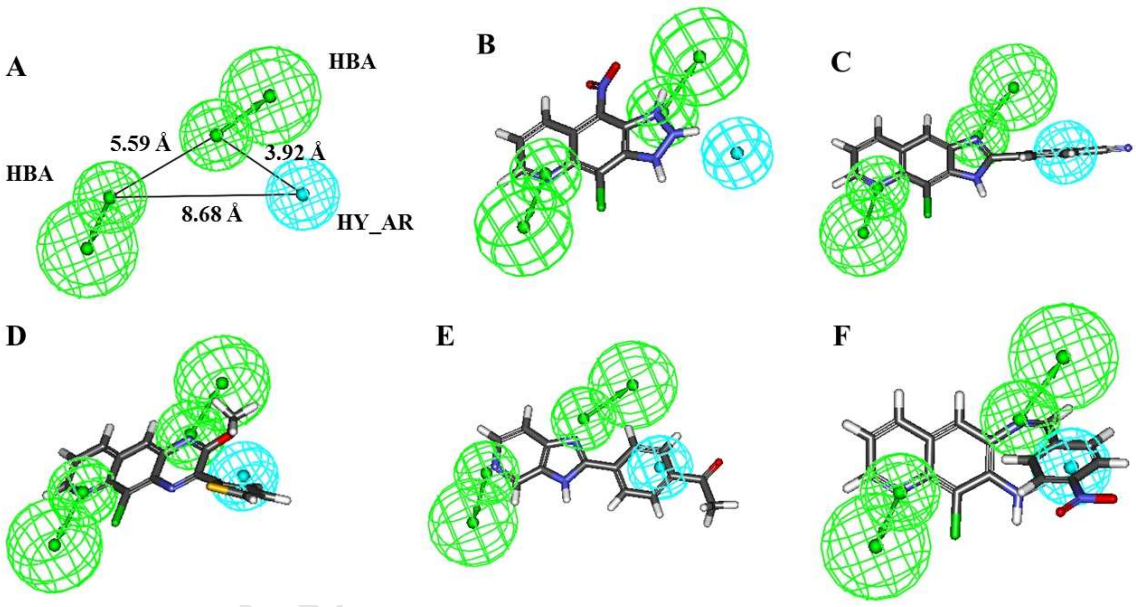

Fig. 7. Geometrical relationships (A) among the features of the top-scoring 3D pharmacophore Hypo1, and pharmacophore mapping of the training set compounds **B1** (B), **6b** (C), **D2** (D), **E2** (E), and **F2** (F). The hypothesis features are portrayed as meshed spheres, color-coded as follows: cyan, HY_AR; green, HBA.

In the successive step, taking advantage of (*i*) the ligand-binding pharmacophoric requirements determined above, and (*ii*) the binding mode of compound **D2** onto the BVDV RdRp described in our previous work,[25] we docked and scored the free energy of binding ΔG_{bind} for compounds

B1, **6b**, **E2**, and **F2** towards the viral target protein, using these 4 additional compounds (together with **D2**) as proofs-of-principle.

Briefly, for compound **D2** we already located a putative binding pocket located between the BVDV RdRp fingers domains 1 and 2 (residues 139–313 and 351–410, respectively).[25] By applying a consolidated molecular dynamic (MD) computational recipe,[27, 28] some specific interactions between the pyridoquinoxaline derivative **D2** and the critical RdRp binding site residues were identified. In details, the aromatic portions of **D2** are encased in two receptor cavities comprising residues A221, I261, I287, Y289 and V216, Y303, V306, K307, P408 and A412, respectively. Moreover, two stable hydrogen bonds (HBs) were detected between the N-pyrido and the quinoxaline nitrogen atom of **D2** and the donor atoms of the side chains of R295 and Y674 of the BVDV RdRp, respectively (Fig. 8). For the record, the thiophene ring of **D2** was involved - through its sulfur atom - in a further HB with S411; however, since the strength of this additional HB was weaker compared to the other two polar interactions,[25] it was classified as a secondary requirement for binding optimization.

Therefore, a thorough search for a residue sequence satisfying the 3D pharmacophoric requirements described above was performed and successfully retrieved in this specific protein region. As clearly shown in Fig. 8, the three features identified by our 3D pharmacophore model find the corresponding counterparts in the binding mode interactions collected by the MD procedure.

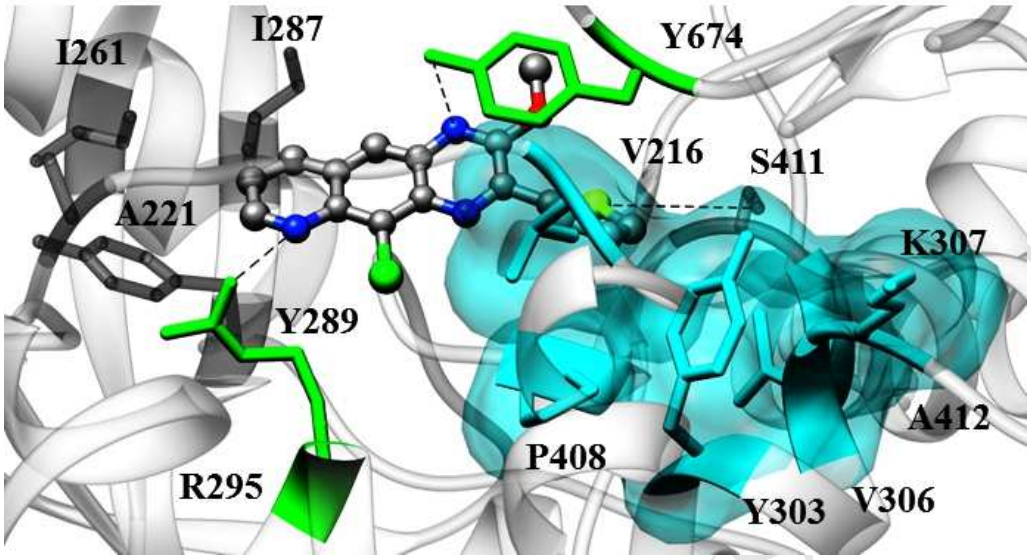

Fig. 8. Equilibrated MD snapshot of the RdRp of BVDV in complex with **D2**.

The image is a zoomed view of the polymerase binding site. The ligand is portrayed in atom-colored sticks-and-balls (gray, C; blue, N; green, Cl; yellow, S), while the secondary structure of the protein is shown as a gray transparent ribbon. The residues satisfying the 3D pharmacophoric requirements in the interaction with **D2** are evidenced as green (HBA) and cyan (HY_AR) sticks and labeled. The cyan area represents the hydrophobic cavity in the protein binding site which encases the heterocyclic moiety of the compound (see Fig. 6). Dark gray labeled residues in sticks within the dark gray area represent the second protein hydrophobic cavity next to the pyridoquinoxaline ring of **D2**. Hydrogen atoms, water molecules, ions and counterions are omitted for clarity.

In the light of these encouraging results, following the same procedure, compounds **B1**, **6b**, **E2**, and **F2** were also docked and scored for affinity towards the binding site of the BVDV RdRp. Pleasingly, for each compound a solution was found in the corresponding set of docked ligand conformations that best reproduced the key 3D pharmacophore requirements, as shown in Fig. 9. Each resulting receptor/ligand complex was then relaxed by energy minimization, followed by MD simulations. Finally, the relevant values of the free energy of binding ΔG_{bind}

between all compounds and the polymerase were evaluated by applying the molecular mechanics/Poisson−Boltzmann surface area (MM/PBSA) computational ansatz (see Computational Details), as listed in Table 2.

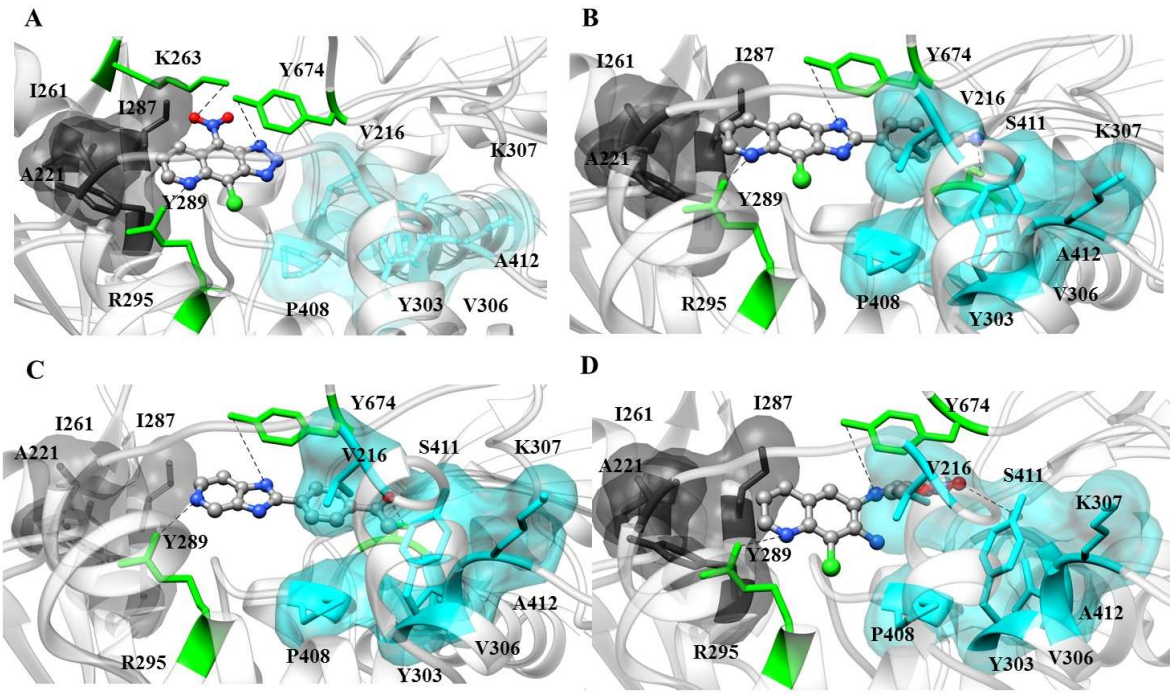

Fig. 9. Equilibrated MD snapshot of the RdRp of BVDV in complex with **B1**, **6b**, **E2**, and **F2**.

The image is a zoomed view of the polymerase binding site. Ligands are portrayed in atom-colored sticks-and-balls (gray, C; blue, N; green, Cl; yellow, S), while the secondary structure of the protein is shown as a gray transparent ribbon. The residues satisfying the 3D pharmacophoric requirements in the interaction with **D2** are evidenced as green (HBA) and cyan (HY_AR) sticks and labeled. The cyan area represents the hydrophobic cavity in the protein binding site which encases the phenyl/heterocyclic moiety of the compounds (see Fig. 6). Dark gray labeled residues in sticks within the dark gray area represent the second protein hydrophobic cavity next

to the pyridoquinoxalinic ring of the compounds. Hydrogen atoms, water molecules, ions and counterions are omitted for clarity. The intensity of the surface color for the hydrophobic cavities is proportional to the corresponding strength of ligand/protein interactions.

Table 2. Free energy components (ΔH_{bind} and $-T\Delta S_{bind}$) and total binding free energies (ΔG_{bind}) for compounds **D2**, **B1**, **6b**, **E2**, and **F2** in complex with the BVDV RdRp. The $IC_{50(calcd)}$ values were obtained from the corresponding ΔG_{bind} values using the relationship: $\Delta G_{bind} = -RT\ln(1/IC_{50})$.

Compound	ΔH_{bind} (kcal/mol)	$-T\Delta S_{bind}$(kcal/mol)	ΔG_{bind}(kcal/mol)	$IC_{50(calcd)}$(μM)
D2	-21.56(0.17)	13.37(0.25)	-8.19(0.30)	0.99
B1	-19.75(0.15)	12.40(0.19)	-7.32(0.24)	4.3
6b	-22.09(0.15)	13.68(0.26)	-8.41(0.26)	0.69
E2	-20.42(0.16)	12.96(0.21)	-7.46(0.25)	3.5
F2	-21.48(0.17)	13.39(0.19)	-8.09(0.25)	1.2

Our qualitative and quantitative computational analysis confirms the experimental trend in terms of correlation between binding capability and inhibitor activity against the viral polymerase. Indeed, all tested compounds exhibit a good affinity against their target protein in the sub- and low-micromolar range (Table 2). Moreover, these molecules share a common binding mode, although slight differences are found for compounds **B**1 and **E2**, as expected. In fact, from their mapping onto the 3D pharmacophore model it could be anticipated that, at variance with the other ligands, both these compounds would not perfectly map all molecular requirements, although for two opposite reasons. The triazoloquinoline derivative **B1**, lacking a bulky aromatic substituent on the 5-membered ring, cannot fill the second hydrophobic cavity of

the protein binding site; however, it can partially compensate this missing interaction by establishing a further H-bond with the side chain of K263 (Fig. 9A). On the other hand, the smaller dimensions of the heterocyclic scaffold of imidazopyridine **E2** does not allow this compound to assume an optimal conformation in the binding site; consequently **E2** cannot perform stable interactions within the first hydrophobic cavity (Fig. 9C). Conversely, the new imidazoquinoline derivative **6b** and the N-benzylidenequinolinamine **F2**, featuring a distribution of functional groups similar to **D2**, fit very well all the pharmacophore requirements (Fig.s 9B and 9D); as a result, their optimal binding conformations reflect into highly favorable ΔG_{bind} values (Table 2).

MD results are further corroborated by the quantitative analysis of the H-bonds between the compounds and the polymerase amino acids mainly involved in binding (Table S3) and by a per-residue deconvolution of the enthalpic contribution to binding afforded by each single residue of the BVDV binding site (Fig. 10). To facilitate reading, the values of $\Delta H_{bind,res}$ for the critical RdRp residues are clustered according to a specific underlying interaction type as follows: A221, I261, I287, and Y289 belong to the first hydrophobic cavity (HC1), and are considered for hydrophobic and π-interactions. Analogously, amino acids V216, Y303, V306, K307, P408, and A412 are clustered in the alternative hydrophobic cavity (HC2), and considered for analogous interaction types.

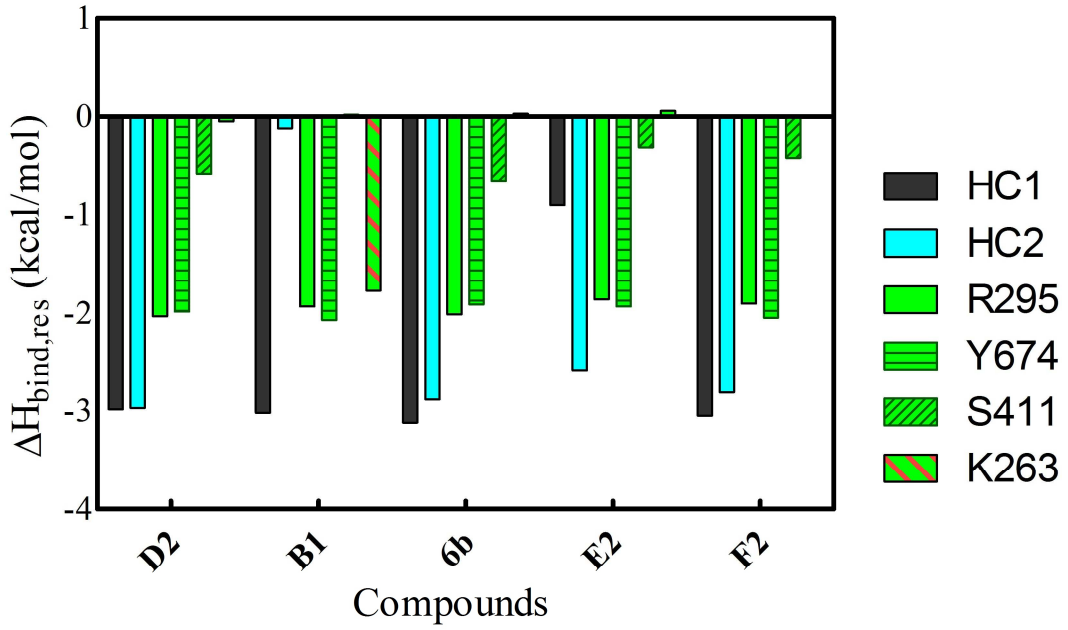

Fig. 10. Per-residue binding enthalpy decomposition $\Delta H_{bind,res}$ for compounds **D2**, **B1**, **6b**, **E2**, and **F2** in complex with the BVDV RdRp.

The collected data support the indications derived from the overall MM/PBSA energetic analysis: the best compounds **D2**, **6b**, and **F2** have indeed quite similar interaction spectra as the main H-bonds involving residues R295 and Y674 persist during the entire simulation trajectory, and their contribution to binding amount to the substantial value of -2 kcal/mole for each amino acid (Fig. 10). Furthermore, the aromatic moiety of the molecules are harbored in both hydrophobic cavities HC1 and HC2; accordingly, the overall corresponding interactions afford an extensive favorable contribution to binding, equal to $\Delta H_{bind,res}$= -5.95 kcal/mol, -6.00 kcal/mol, and -5.86 kcal/mol for **D2**, **6b**, and **F2**, respectively (Fig. 10). Finally, even the small stabilization afforded by the supplementary H-bond with S411 is confirmed by the energy decomposition analysis.

In this scenario, our computational approach allows to better understand the reasons of the low yet significant inhibitory efficacy of the two remaining compounds **B1** and **E2**. Although the $\Delta H_{bind,res}$ value of the interaction of the triazoloquinoline derivative with the HC2 residues is essentially negligible (-0.12 kcal/mol, Fig. 10), the presence of the permanent H-bond, with an Average Dynamic Length (ADL) of 1.99 ± 0.05 Å, detected between the nitro group of **B1** and the side chain of K263 partially offsets this contribution; concomitantly, the interactions of **B1** with the side chains of residues lining the HC1 are comparable to the ones characterizing the best binder (Fig. 10). The binding mode of the imidazopyridine **E2**, instead, satisfies the same requisites underlying the binding of best RdRp inhibitors; however, its smaller scaffold is not able to preserve the same intensity in these interactions, particularly in the case of the hydrophobic contribution from HC1 ($\Delta H_{bind,res}$ = -0.90 kcal/mol, Fig. 10).

The computational results discussed above yielded a precise scheme of the principal intermolecular interactions sustaining the binding between the BVDV RdRp and the present, specific classes of its inhibitors. To validate these indications we next performed a combined *in silico/in vitro* mutagenesis study of those protein residues involved in the binding site, mainly via highly stabilizing H-bonds with the ligands (Fig. 10). To this purpose, the following polymerase residues: R195, Y674 (two key ligand/protein anchor points for all tested compounds) and K263 (exerting an exclusive role in the binding mode of the triazoloquinoline derivatives **B1**) were all mutated into alanine. Then, the affinity of the mutated viral RdRp towards all compounds **D2**, **B1**, **6b**, **E2**, and **F2** were concurrently evaluated *in silico* and *in vitro*. The aggregate results are listed in Table 3, while all dose–response curves obtained from *in vitro* enzyme assays are showed in Fig. S2.

Table 3. *In vitro/in silico* alanine mutagenesis of the RdRp of BVDV residues K263, R295, and Y674.According to its definition ($\Delta\Delta G_{bind}=\Delta G_{bind(WT)}-\Delta G_{bind(MUT)}$), positive values calculated for $\Delta\Delta G_{bind}$ indicate that the considered amino acid substitution at a given position of BVDV RdRp is favorable in terms of interaction with the inhibitors, whereas negative values indicate that the corresponding mutation is unfavorable to binding. n.e. = not evaluable (see Fig. S2).

Compound	RdRp residue	ΔG_{bind} (kcal/mol)	$\Delta\Delta G_{bind}$ (kcal/mol)	$IC_{50(calcd)}$ (μM)	$IC_{50(exp)}$ (μM)
D2	WT	-8.19 ±0.30	-	0.99	0.64
	K263A	-7.98 ± 0.25	-0.21	1.4	0.96
	R295A	-3.69 ± 0.27	-4.50	2.0×10^3	n.e.
	Y674A	-3.93 ± 0.23	-4.26	1.3×10^3	n.e.
B1	WT	-7.32±0.25	-	4.3	9.0
	K263A	-5.42 ± 0.24	-1.90	107	140
	R295A	-3.75 ± 0.27	-3.57	1.8×10^3	n.e.
	Y674A	-3.59 ± 0.26	-3.73	2.3×10^3	n.e.
6b	WT	-8.41±0.26	-	0.69	0.48
	K263A	-8.32 ± 0.24	-0.09	0.80	0.75
	R295A	-3.83 ± 0.23	-4.58	1.6×10^3	n.e.
	Y674A	-3.99 ± 0.25	-4.42	1.2×10^3	n.e.
E2	WT	-7.46±0.25	-	3.4	11
	K263A	-7.51 ± 0.24	0.05	3.2	15
	R295A	-3.80 ± 0.26	-3.66	1.6×10^3	n.e.
	Y674A	-4.01 ± 0.23	-3.45	1.2×10^3	n.e.
F2	WT	-8.09 ±0.25	-	1.1	0.81
	K263A	-7.91 ± 0.25	-0.18	1.6	1.0
	R295A	-3.87 ± 0.22	-4.22	1.5×10^3	n.e.
	Y674A	-4.11 ± 0.24	-3.98	0.98×10^3	n.e.

Inspection of Table 3 immediately reveals the excellent agreement between computational prediction and experimental determination of IC_{50} values for all compounds considered, this evidence thereby constituting a solid validation of the *in silico* strategy presently adopted. Next, our combined approach was able to dissect the effect of each mutation on the binding strength of all tested compounds against the polymerase, ultimately supporting our description of their binding mode onto the viral protein. In detail, the substitution of the polar residue R295 and Y674 with alanine is predicted to dramatically decrease the BVDV RdRp affinity of all 5 molecules, as testified by the corresponding $\Delta\Delta G_{bind}$ values in Table 3: the loss of at least 3.5 kcal/mol indeed means that these specific residues are very important not only for their single point interaction but also for the overall conformation and stability of the entire polymerase binding site. Since the exerted effect of the two mutations is comparable for all 5 compounds, for the sake of brevity we will discuss here in details the results achieved for the mutated proteins in complex with the new imidazoquinoline derivatives **6b**. The top panel of Fig. S3 nicely shows how the binding site for this compound is deeply affected by both R295A and Y674A mutations: the absence of the relevant drug/protein H-bonds forces the compound to adopt a different conformation upon binding and this, in turn, reflects into a general weakening of the entire network of stabilizing intermolecular interactions.

In keeping, the calculated ΔG_{bind} values plummet from -8.41 kcal/mol for the wild-type protein to -3.83 kcal/mol and -3.99 kcal/mol for the R295A and Y674A mutant polymerases, respectively (Table 3). Consistently, the relevant $IC_{50(calcd)}$ values increase more than 4 orders of magnitude, reaching values as high as $1.6 \times 10^3 \mu M$ (R295A) and $1.2 \times 10^3 \mu M$ (Y674A). The compound activity tested *in vitro* parallels this computational prediction: indeed, the BVDV

RdRp inhibitory activity of **6b** at all compound concentrations considered was so low that the corresponding $IC_{(50,exp)}$ could not be determined (Table 4 and Fig. S2).

Lastly, the BVDV RdRp K263A mutant protein was studied with the purpose of and validating the specific binding mode predicted for compound **B1**; as such, lysine residue 263 in fact does not constitute a topic molecular determinant for the polymerase binding of any other compounds considered. In fact, taking again derivative **6b** as proof-of-concept, mutating K into A at that position results in a negligible modification of the drug binding configuration and intermolecular interactions (Fig. S3C) and, hence, in the corresponding ΔG_{bind} value (Table 3). On the contrary, for compound **B1** this anchor point instrumental to protein binding is lost in the presence of the A623 mutation (Fig. S3D), and the calculated affinity against the BVDV RdRp plunges one order of magnitude, i.e., from -7.32 kcal/mol for the WT to -5.42 kcal/mol for the K632A mutant (Table 3). Accordingly, the predicted and experimental IC_{50}s both increase from a low micromolar value for the WT ($IC_{(50,calcd)}$ = 4.3 μM and $IC_{(50,exp)}$ = 9.0 μM) to > 100μM for the K263A mutated protein($IC_{(50,calcd)}$ = 107μM and $IC_{(50,exp)}$ = 140μM), as shown in Table 3 and Fig. S2.

Conclusions

In our long-standing research activity in the design, synthesis, characterization, and testing of antiviral compounds towards viruses of the *Flavivirus* genera, we produced a plethora of molecular classes among which several compounds were found concomitantly endowed with high potency towards BVDV and negligible toxicity.

Along our antiviral research activity, linear aromatic N-tricyclic systems emerged for their interesting anti-*Flaviviridae* activity. From the combination of the quinoline nucleus with 1,2,3-

triazole, imidazole or pyrazine, best results were obtained for imidazo[4,5-g]quinoline derivatives as anti-BVDV agents. In this paper we expanded the SAR analysis through rational modifications of lead compound 2-phenyl-3*H*-imidazo[4,5-g]quinoline **C1** (EC_{50} = 4 μM, CC_{50} > 100 μM).

Diverse substituents at positions R_1, R_2, and/or R_3 of proposed model in Fig. 6, and replacement of phenyl ring with a furane moiety led to 12 new imidazo[4,5-g]quinoline derivatives. Influence on the anti-BVDV activity of the Cl atom at position R_1, of steric hindrance of substituents in R_2, of electron donating groups (EDGs) or electron withdrawing groups (EWGs) on the phenyl group (R_3 in Fig. 6) and of heterocyclic moiety on quinoline scaffold was evaluated.

The SAR analysis of this molecular series highlighted how the combined presence of a chlorine substituent and an electron withdrawing group such as –CN on position 4′ of phenyl moiety retains and enhances the antiviral activity of the corresponding derivative compared to the lead compounds **C1**. From this series, compound **6b** emerged as new lead compound, showing EC_{50} value of 0.3 μM and S.I. > 333.3.

With the purpose of finding a sensible molecular rationale underlying the common affinity towards the RdRp BDVD of these different molecular classes, we then performed a jointed *in silico*/*in vitro* study. To the purpose, we started with the development of a common-feature three-dimensional pharmacophore model, which allowed us to determine two H-bond acceptors and one aromatic hydrophobic feature as the fundamental interactions leading to efficient drug/protein binding. Exploiting this information, the binding site and the binding mode of all 5 classes of compounds onto the BVDV RdRp were retrieved; next, the activity of all compounds was scored using the MM/PBSA approach, obtaining a good agreement between calculated free

energies of binding ΔG_{bind} and the corresponding experimental EC_{50} values. The per residue deconvolution of the enthalpic component of ΔG_{bind} identified two RdRp amino acids – namely R295 and Y674, as the two fundamental H-bond donors, while two hydrophobic cavities HC1 (residues A221, I261, I287, and Y289) and HC2 (residues V216, Y303, V306, K307, P408, and A412) were determined to fulfill the third pharmacophoric requirement. Bases on this information, three RdRp residues critical for drug binding were selected and mutagenized, both *in silico* and *in vitro*, into alanine, and the affinity of a set of selected compounds towards the mutant RdRp isoforms was determined accordingly. The agreement between predicted and experimental data confirmed the proposed common molecular rationale shared by molecules characterized by different chemical scaffolds in binding to the BVDV RdRp.

Ultimately, the information yielded by our combined *in silico/in vitro* approach could provide an interesting tool for the efficient development of new, powerful compounds against this important *Pestivirus*.

Experimental Section

General directions. Melting points are uncorrected and were measured in open capillaries in a Digital Electrothermal IA9100 melting point apparatus. ^{1}H NMR spectra were recorded on a Varian BrukerAvance II 600-MHz spectrometer, using TMS as internal standard. The chemical shift values are reported in ppm (δ) and coupling constants (J) in Hertz (Hz). Signal multiplicities are represented by: s (singlet), d (doublet), dd (double doublet), t (triplet), q (quadruplet) and m (multiplet). Column chromatography was performed using 70-230 mesh (Merck silica gel 60). Light petroleum refers to the fraction with b.p. 40-60°C. TLC using Merck F-254 commercial

plates monitored the progress of the reactions and the Rf. Analyses indicated by the symbols of the elements were within ± 0.4 % of the theoretical values. Chromatographic separation was performed on an Agilent 1100 LC System that included a binary pump, Diode-Array Detector, column thermostat, degasser, and HTS-PAL autosampler (Agilent Technologies, Paolo Alto, CA, USA). The HPLC column was a Luna C18 (2) (4.6 · 150 mm, 3 μm) from Phenomenex (Torrance, CA, USA) with a security guard cartridge (4 · 2 mm). The mobile phase consisted of Eluent A (water with 0.1% acetic acid) and Eluent B (acetonitrile). The flow rate was set to 0.5 mL/min and the column temperature was 33 °C. Total run time was 30 min. The gradient program is shown in Table S2 (see Supporting Information).

General procedure for the preparation of imidazo[4,5-g]quinolines 2-5a, **6-11b**, **12-13c**, **and 14b.**

Following a previously established procedure [23], compounds **2-5a**, **6-11b**, **12-13c**, and **14b** were synthesized by condensation of the diaminoquinolines **1a–c** (1–3 mmol) with an equimolar amount of the suitable activated aldehyde (Bertagnini's salt), in refluxed ethanol (10–30 mL) for 8 h or in DMF (dimethylformamide) at 130 °C for 2-12 h. All Bertagnini's salts were obtained in high yields from the commercially available corresponding aldehydes (Aldrich) with $Na_2S_2O_5$ in ethanol, according to the procedure used by Shriner and Land [29].

On cooling, a small amount of inorganic compound was filtered off and the ethanol mother liquors were evaporated to dryness *in vacuo*. The solid residues, colored from orange to dark red, were purified by recrystallization from ethanol in good yields. Compound 4-(4-chloro-3H-imidazo[4,5-g]quinolin-2-yl)benzenesulfonamide (**11b**) was prepared by condensation of the diaminoquinoline **1b** (1.03 mmol) with an equimolar amount of 4-sulfamoylbenzoic and

polyphosphoric acid (8.0 g) for 4 h at 200 °C. On cooling, the mixture reaction was poured into 100 mL of water and the pH brought to 5 with 10 M NaOH. The resulting precipitate was filtered off and washed with water obtaining **11b** in 25% yield.

4-(3*H*-imidazo[4,5-*g*]quinolin-2-yl)benzonitrile (2a). Solvent: ethanol. Time of reaction: 8 h. Yield: 52%. M.p. > 300 °C. ^{1}H NMR ($CDCl_3$ + DMSO-d_6): δ 9.01 (d, 1H, J = 4.2 Hz, H-6), 8.85 (d, 1H, J = 8.2 Hz, H-8), 8.70–8.40 (m, 4-phenyl H), 8.26 (s, 1H, H-4), 8.15 (s, 1H, H-9), 7.74 (d, 1H, J = 8.2 Hz, H-7).LC/MS: 271 (M+H). Anal.Calcd.for ($C_{17}H_{10}N_4$): C, 75.54; H, 3.73; N, 20.73. Found: C, 75.35; H, 3.64; N, 20.87.

2-(4-(trifluoromethyl)phenyl)-3*H*-imidazo[4,5-*g*]quinoline (3a). Solvent: ethanol. Time of reaction: 8 h. Yield: 86%. M.p. > 300 °C. ^{1}H NMR ($CDCl_3$ + DMSO-d_6): δ 9.10-9.16 (m, 2H, H-7 and H-5), 8.65 (s, 1H, H-4), 8.58 (d, 2H, J = 8.0 Hz, H-2′, H-6′), 8.54 (s, 1H, H-9), 7.80-7.90 (m, 3H, H-3′, H-5′, H-6). LC/MS: 314 (M+H). Anal.Calcd.for ($C_{17}H_{10}F_3N_3$): C, 65.18; H, 3.22; F, 18.19; N, 13.41. Found: C, 65.22; H, 3.15; F, 18.17; N, 13.49.

2-(2,4-dimethoxyphenyl)-3*H*-imidazo[4,5-*g*]quinoline (4a). Solvent: ethanol. Time of reaction: 8 h. Yield: 56%. M.p.: 218 °C. ^{1}H NMR ($CDCl_3$ + DMSO-d_6): δ 9.02 (d, 1H, H = 4.0 Hz, H-7), 8.90 (d, 1H, J = 8.0, H-5), 8.30-8.40 (m, 3H, H-4, H-9, H-6′), 7.68 (dd, 1H, J = 8.2 and J = 4.0, H-6), 6.80-6.70 (m, 2H, H-3′, H-5′), 4.13 (s, 3H, OCH_3), 3.92 (s, 3H, OCH_3). LC/MS: 306 (M+H). Anal.Calcd.for ($C_{18}H_{15}N_3O_2$): C, 70.81; H, 4.95; N, 13.76. Found: C, 70.69; H, 5.11; N, 13.67.

2-(2,4-difluorophenyl)-3*H*-imidazo[4,5-*g*]quinoline (6a). Solvent: ethanol. Time of reaction: 8 h. Yield: 46%. M.p. > 300 °C. ^{1}H NMR ($CDCl_3$ + DMSO-d_6): δ 12.47 (s, 1H, NH), 8.90-8.80 (m, 1H, H-7), 8.54-8.02 (m, 3H, H-4, H-5, H-6′), 7.72 (s, 1H, H-9), 7.36 (dd, 1H, J = 8.4 and J =

4.0 Hz, H-6), 7.19-7.11 (m, 2H, H-3′, H-5′). LC/MS: 282 (M+H). Anal.Calcd for ($C_{16}H_9F_2N_3$): C, 68.33; H, 3.23; F, 13.51; N, 14.94. Found: C, 68.25; H, 3.17; F, 13.44; N, 15.02.

4-(4-chloro-3*H*-imidazo[4,5-*g*]quinolin-2-yl)benzonitrile (6b). Solvent: DMF. Time of reaction: 4 h. Yield: 90%. M.p. > 300 °C. ^{1}H NMR ($CDCl_3$ + DMSO-d_6): δ8.97 (d, 1H, J = 4.0 Hz, H6), 8.67 (d, 2H, J = 8.0 Hz H-3′, H-5′), 8.42 (d, 2H, J = 8.0 Hz, H-2′, H-6′), 8.16-8.08 (m, 1H, H-8), 8.02 (s, 1H, H-9), 7.49 (dd, 1H, J = 8.2 and 4.0 Hz, H-7). LC/MS: 305 (M+H). Anal.Calcd.for ($C_{17}H_9ClN_4$): C, 67.00; H, 2.98; Cl, 11.63; N, 18.39. Found: C, 67.07; H, 3.03; Cl, 11.70; N, 18.47.

4-chloro-2-(4-(trifluoromethyl)phenyl)-3*H*-imidazo[4,5-*g*]quinoline (7b). Solvent: DMF. Time of reaction: 4 h. Yield: 81%. M.p. > 300 °C. ^{1}H NMR ($CDCl_3$ + DMSO-d_6): δ 8.96 (d, 1H, J = 3.8 Hz,H-6), 8.59 (d, 2H, J = 7.2 Hz, H-2′, H-6′), 8.48 (d, 1H, J = 8.2 Hz, H-8), 8.11 (s, 1H, H-9), 7.89 (d, 2H, J = 7.8 Hz, H-3′, H-5′), 7.48 (dd, 1H, J = 8.0 and J = 4.0 Hz, H-7). LC/MS: 348 (M+H). Anal.Calcd.for ($C_{17}H_9ClF_3N_3$): C, 58.72; H, 2.61; Cl, 10.20; F, 16.39; N, 12.08. Found: C, 58.65; H, 2.54; Cl, 10.24; F, 16.31; N, 12.15.

4-chloro-2-(2,4-dimethoxyphenyl)-3*H*-imidazo[4,5-*g*]quinoline (8b). Solvent: ethanol. Time of reaction: 8 h. Yield: 60%. M.p. 231 °C. ^{1}H NMR ($CDCl_3$ + DMSO-d_6): δ 8.92 (d, 1H, J = 3.9 Hz, H-6), 8.55 (d, 1H, J = 8.2 Hz, H-8), 8.45 (d, 1H, J = 8.8 Hz, H-6′), 8.06 (s, 1H, H-9), 7.49 (dd, 1H, J = 8.0 and J = 4.0 Hz, H-7), 6.82-6.79 (m, 2H, H-3′, H-5′), 4.08 (s, 3H, OCH_3), 3.90 (s, 3H, OCH_3). LC/MS: 340 (M+H). Anal.Calcd.for ($C_{18}H_{14}ClN_3O_2$): C, 63.63; H, 4.15; Cl, 10.43; N, 12.37. Found: C, 63.57; H, 4.09; Cl, 10.37; N, 12.41.

1-(4-(4-chloro-3*H*-imidazo[4,5-*g*]quinolin-2-yl)phenyl)ethanone (9b). Solvent: DMF. Time of reaction: 2 h. Yield: 85%. M.p. > 300 °C. ^{1}H NMR ($CDCl_3$ + DMSO-d_6): δ 8.97 (d, 1H, J = 4.2 Hz, H-6), 8.43 (d, 1H, J = 8.4 Hz, H-8), 8.52 (d, 2H, J = 8.4 Hz, H-3′, H-5′), 8.13 (d, 2H, J =

8.4 Hz, H-2′, H-6′), 8.06 (s, 1H, H-9), 7.47 (dd, 1H, J = 8.6 and J = 4.2 Hz, H-7) , 2.68 (s, 3H, CH_3). LC/MS: 322 (M+H). Anal.Calcd.for ($C_{18}H_{12}ClN_3O$): C, 67.19; H, 3.76; Cl, 11.02; N, 13.06. Found: C, 67.15; H, 3.70; Cl, 11.08; N, 13.12.

4-chloro-2-(4-(methylthio)phenyl)-3*H*-imidazo[4,5-*g*]quinoline (10b). Solvent: DMF. Time of reaction: 2 h. Yield: 73%. M.p. 298 °C. ^{1}H NMR ($CDCl_3$ + DMSO-d_6): δ 8.93 (d, 1H, J = 4.2 Hz, H-6), 8.52 (d, 1H, J = 7.6 Hz, H-8), 8.30 (d, 2H, J = 8.6 Hz, H-3′, H-5′), 8.07 (s, 1H, H-9), 7.51 (dd, 1H, J = 7.6 and J = 4.2 Hz, H-7), 7.44 (d, 2H, J = 8.6 Hz, H-2′, H-6′), 2.58 (s, 3H, CH_3). LC/MS: 326 (M+H). Anal.Calcd.for ($C_{17}H_{12}ClN_3S$): C, 62.67; H, 3.71; Cl, 10.88; N, 12.90; S, 9.84. Found: C, 62.72; H, 3.78; Cl, 10.80; N, 12.85; S, 9.89.

4-(4-chloro-3*H*-imidazo[4,5-*g*]quinolin-2-yl)benzenesulfonamide (11b). Yield: 25%.M.p. > 300 °C. ^{1}H NMR ($CDCl_3$ + DMSO-d_6): δ 9.40 (dd, 1H, J = 4.2 and J = 1.8 Hz, H-6), 8.51 (dd, 1H, J = 8.0 and J = 1.8 Hz, H-8), 8.35 (d, 2H, J = 8.2 Hz, H-3′, H-5′), 8.10 (s, 1H, H-9), 7.89 (d, 2H, J = 8.4 Hz, H-2′, H-6′), 7.49 (dd, 1H, J = 8.4 and J = 3.8 Hz, H-7). LC/MS: 359 (M+H). Anal.Calcd.for ($C_{16}H_{11}ClN_4O_2S$): C, 53.56; H, 3.09; Cl, 9.88; N, 15.61; S, 8.94. Found: C, 53.62; H, 3.13; Cl, 9.83; N, 15.67; S, 9.01.

4-chloro-3-(cyclohexylmethyl)-2-(4-methoxyphenyl)-3*H*-imidazo[4,5-*g*]quinoline (12c). Solvent: DMF. Time of reaction: 2 h. Yield: 22%. M.p. 77 °C. ^{1}H NMR ($CDCl_3$ + DMSO-d_6): δ 9.05 (dd, 1H,J = 4.2 and J = 1.8 Hz, H-6), 8.36 (dd, 1H, J = 8.4 and J = 1.6 Hz, H-8), 8.16 (s, 1H, H-9), 7.70 (d, 2H, J = 9.2 Hz, H-2′, H-6′), 7.44 (dd, 1H, J = 8.6 and J = 4.2 Hz, H-7), 7.09 (d, 2H, J = 8.8 Hz, H-3′, H-5′), 4.58 (2H, d, J = 6.8 Hz, CH_2), 3.92 (s, 3H, CH_3), 1.95-0.83 (m, 11H, cyclohexyl). LC/MS: 407 (M+H). Anal.Calcd.for ($C_{24}H_{24}ClN_3O$): C, 71.01; H, 5.96; Cl, 8.73; N, 10.35. Found: C, 71.10; H, 6.06; Cl, 8.69; N, 10.28.

4-chloro-3-(cyclohexylmethyl)-2-(4-nitrophenyl)-3*H*-imidazo[4,5-*g*]quinoline (13c). Solvent: DMF. Time of reaction: 12 h. Yield: 20%. M.p. 228 °C. ^{1}H NMR ($CDCl_3$ + DMSO-d_6): δ 9.10 (dd, 1H,J = 4.2 and J = 1.8 Hz, H-6), 8.46 (d, 2H, J = 9.2 Hz, H-2′, H-6′), 8.40 (dd, 1H, J = 8.4 and J = 1.6 Hz, H-8), 8.24 (s, 1H, H-9), 7.98 (d, 2H, J = 8.8 Hz, H-3′, H-5′), 4.48 (dd, 1H, J = 8.4 and J = 4.2 Hz, H-7), 4.56 (2H, d, J = 6.8 Hz, CH_2), 1.95-0.82 (m, 11H, cyclohexyl). LC/MS: 421 (M+H). Anal.Calcd.for ($C_{23}H_{21}ClN_4O_2$): C, 65.63; H, 5.03; Cl, 8.42; N, 13.31. Found: C, 65.58; H, 4.98; Cl, 8.41; N, 13.36.

4-chloro-2-(furan-3-yl)-3*H*-imidazo[4,5-*g*]quinoline (14b). Solvent: ethanol. Time of reaction: 8 h. Yield: 86%. M.p.> 300 °C. ^{1}H NMR ($CDCl_3$ + DMSO-d_6): δ 8.96 (dd, 1H, J = 4.2 and J = 1.4 Hz, H-6), 8.60 (dd, 1H, J = 1.6 and J = 0.8 Hz, H-2′), 8.47 (dd, 1H, J = 8.2 and J = 1.2 Hz, H-8), 8.04 (s, 1H, H-9), 7.72 (dd, 1H, J = 3.6 Hz and J = 2.0 Hz, H-4′), 7.49 (dd, 1H, J = 8.6 and J = 4.2 Hz, H-7), 7.26 (dd, 1H, J = 1.6 and J = 0.8 Hz, H-5′). LC/MS: 270 (M+H). Anal.Calcd.for ($C_{14}H_8ClN_3O$): C, 62.35; H, 2.99; Cl, 13.15; N, 15.58. Found: C, 62.42; H, 3.04; Cl, 13.10; N, 15.53.

Biology

Test compounds

Compounds were dissolved in DMSO at 100 mM and then diluted in culture medium.

Cells and viruses

Cell lines were purchased from American Type Culture Collection (ATCC). The absence of mycoplasma contamination was checked periodically by the Hoechst staining method. Cell lines supporting the multiplication of RNA and DNA viruses were the following: Madin Darby Bovine Kidney (MDBK) [ATCC CCL22 (NBL-1) *Bos taurus*], Baby Hamster Kidney (BHK-21) [ATCC CCL10 (C-13) *Mesocricetusauratus*] and Monkey kidney (Vero 76) [ATCCCRL 1587

CercopithecusAethiops]. Viruses were purchased from American Type Culture Collection (ATCC), with the exception of Yellow Fever Virus (YFV). Viruses representative of positive-sense single stranded RNAs (ssRNA^{+}) were: (i) *Flaviviridae*: yellow fever virus (YFV) [strain 17-D vaccine (Stamaril Pasteur J07B01)] and bovine viral diarrhea virus (BVDV) [strain NADL (ATCC VR-534)]; (ii) *Picornaviridae*: human enterovirus B [coxsackie type B5 (CV-B5), strain Faulkner, (ATCC VR-185)], and human enterovirus C [poliovirus type-1 (Sb-1), Sabin strain Chat (ATCC VR-1562)]. Viruses representative of negative-sense, single-stranded RNAs (ssRNA−) were: (i) *Paramyxoviridae*: human respiratory syncytial virus (RSV) [strain A2 (ATCC VR-1540)]; (ii) *Rhabdoviridae*: vesicular stomatitis virus (VSV) [lab strain Indiana (ATCC VR 158)]. The virus representative of double-stranded RNAs (dsRNA) *Reoviridae* was reovirus type-1 (Reo-1) [simian virus 12, strain 3651 (ATCC VR- 214)]. DNA virus representatives was *Poxviridae*: vaccinia virus (VV) [strain Elstree (Lister Vaccine) (ATCC VR-1549)].

Cytotoxicity assays

Cytotoxicity assays were run in parallel with antiviral assays. MDBK and BHK cells were seeded in 96-well plates at an initial density of 6×10^5 and 1×10^6 cells/mL, respectively, in Minimum Essential Medium with Earle's salts (MEM-E), l-glutamine, 1 mM sodium pyruvate and 25 mg/L kanamycin, supplemented with 10% horse serum (MDBK) or 10% fetal bovine serum (FBS) (BHK). Cell cultures were then incubated at 37 °C in a humidified, 5% CO_2 atmosphere in the absence or presence of serial dilutions of test compounds. Cell viability was determined after 72 hrs at 37 °C by the 3-(4,5- dimethylthiazol-2-yl)-2,5-diphenyl-tetrazolium bromide (MTT) method.[30] Vero-76 cells were seeded in 96-well plates at an initial density of 4×10^5 cells/mL, in Dulbecco's Modified Eagle Medium (D-MEM) with l-glutamine and 25 mg/L kanamycin, supplemented with 10% FBS. Cell cultures were then incubated at 37 °C in a humidified, 5% CO_2 atmosphere in the absence or presence of serial dilutions of test compounds. Cell viability was determined after 48–96 hrs at 37 °C by the MTT method.

Antiviral assays

Antiviral activity against YFV and Reo-1 was based on inhibition of virus-induced cytopathogenicity in BHK-21 cells acutely infected with a m.o.i. of 0.01. Activity of compounds activity against BVDV was based on inhibition of virus-induced cytopathogenicity in MDBK cells acutely infected with a m.o.i. of 0.01. Briefly, BHK and MDBK cells were seeded in 96-well plates at a density of 5×10^4 and 3×10^4 cells/well, respectively, and were allowed to form confluent monolayers by incubating overnight in growth medium at 37 °C in a humidified CO_2 (5%) atmosphere. Cell monolayers were then infected with 50 µL of a proper virus dilution in maintenance medium [MEM-Earl with l-glutamine, 1 mM sodium pyruvate and 0.025 g/L kanamycin, supplemented with 0.5% inactivated FBS] to give an m.o.i of 0.01. After 2 hrs, 50 µL of maintenance medium, without or with serial dilutions of test compounds, were added. After a 3-/4-day incubation at 37 °C, cell viability was determined by the MTT method [39].

Antiviral activity against CVB-5, Sb-1, RSV, VSV and VV was determined by plaque reduction assays in infected cell monolayers. To this end, Vero 76-cells were seeded in 24-well plates at a density of 2×10^5 cells/well and were allowed to form confluent monolayers by incubating overnight in growth medium [Dulbecco's Modified Eagle Medium (D-MEM) with l-glutamine and 4500 mg/L d-glucose and 0.025 g/L kanamycin, supplemented with 10% FBS] at 37 °C in a humidified CO_2 (5%) atmosphere. Then, monolayers were infected for 2 hrs with 250 µL of proper virus dilutions to give 50 to 100 PFU/well. Following removal of unadsorbed virus, 500 µL of maintenance medium [D-MEM with l-glutamine and 4500 mg/L d-glucose, supplemented with 1% inactivated FBS] containing 0.75% methylecellulose, without or with serial dilutions of test compounds, were added. Cultures were incubated at 37 °C for 2 (Sb-1 and VSV), 3 (CVB-5, and VV) or 5 days (RSV) and then fixed with PBS containing 50% ethanol and 0.8% crystal violet, washed and air-dried. Plaques were then counted.

Linear regression analysis

The extent of cell growth/viability and viral multiplication, at each drug concentration tested, were expressed as percentage of untreated controls. Concentrations resulting in 50% inhibition (CC_{50} or EC_{50}) were determined by linear regression analysis.

Computational Details

Pharmacophore Modeling. The purpose of the present work is not using the HipHop derived pharmacophore model *tout court* for designing new compounds but as a tool for guiding and refining the docking of the selected 31 compounds of all series into the relevant binding site of the BVDV RdRp. Accordingly, four different molecular scaffolds were chosen to ensure a certain degree of structural variety; accordingly, 9 pyridoquinoxalines from series **D**, 15 imidazoquinolines, of which 5 from series **C** and 10 new compounds **2-4a**, **6-10b**, **13c**, and **14b**, 2 triazolquinolines from series **B**, and 5 molecules belonging to the **E** and **F** series. A principal value (PV) of 2 was assigned to the most active compounds in the training set (EC_{50} values <5μM), whereas PV = 1 was assigned for compounds with the inhibitory activity in the range between 5 μM and 99μM and PV = 0 was attributed to inactive molecules ($EC_{50} \geq 100$μM, Table S2). Compound models energy minimization was performed with the CHARMM forcefield[31] and the classical conformational search was carried out using the Poling algorithm[32] as implemented in the *Catalyst* module of Discovery Studio.[33] All 23 training set compounds associated with their best conformations were used in the common feature pharmacophore generation using the *HipHop* feature of *Catalyst*. As suggested by the inhibitor chemical scaffolds, the hydrogen bond acceptor (HBA), hydrophobic (HY), hydrophobic aromatic (HY_AR), and ring aromatic (RA) features were selected for pharmacophore construction.

The top-ten qualitative pharmacophore models were developed to identify the common features required for efficient BVDV RdRp inhibition, whilst cluster analysis was used to evaluate and categorize differences between composition and spatial location of the chemical features of the models. On the basis of the pharmacophoric features presented, all resulting models could be roughly classified into two major clusters. The first seven models in cluster I

identified three functional features, including two HBAs and one HY_AR. The three models in cluster II recognized other functional features, with one HBA, one HY_AR, and one RA. The distances between the pharmacophoric features in cluster I models were rather constant, with little difference in their ranking score; consequently, an analysis of the best fit values of the training set compounds was carried out to determine the best model.

Molecular Dynamics simulation.

The optimized structures of selected compounds **B1**, **6b**, **E2**, and **F2** were docked into the BVDV RdRp binding pocket using the optimized structure of the RdRp of BVDV taken from our previous work.[25, 27, 28] All docking experiments were performed with Autodock 4.3/AutodockTools 1.4.6[34] on a win64 platform. The inhibitor/RdRp complex obtained from the docking procedure was further refined in Amber 14[35] as previously described.[25, 27, 28] Accordingly, the best energy configuration of each complex wassubsequently solvated by a cubic box of TIP3P[36] water molecules extending at least 10 Å in each direction from the solute. The system was neutralized and the solution ionic strength was adjusted to the physiological value of 0.15 M by adding the required amounts of Na^+ and Cl^- ions. Each solvated system was relaxed by 500 steps of steepest descent followed by 500 other conjugate gradient minimization steps and then gradually heated to a target temperature of 300 K. All simulations were carried out with periodic boundary conditions. Subsequently, the density of the system was equilibrated via MD runs in the isothermal isobaric (NPT) ensemble for 50 ps with a time step of 1 fs, with isotropic position scaling and a pressure relaxation time of 1.0 ps. Eachs system was further equilibrated using NPT MD runs at 300 K, with a pressure relaxation time of 2.0ps. Three equilibration steps were performed, each 4 ns long and with a time step of 2.0 fs. To check the

system stability, the fluctuations of the root-mean-square-deviation (rmsd) of the simulated position of the backbone atoms of the BVDV RdRp protein with respect to those of the initial protein were monitored. All chemico-physical parameters and rmsd values showed very low fluctuations at the end of the equilibration process, indicating that the systems reached a true equilibrium condition. The equilibration phase was followed by a data production run consisting of50 ns of MD simulations in the canonical (NVT) ensemble. Only the last 20 ns of each equilibrated MD trajectory were considered for statistical data collections. A total of 1000 trajectory snapshots were analyzed the each molecule/polymerase complex.

Free energy of binding analysis.

The binding free energy, ΔG_{bind}, between the selected compounds and the BVDV RdRp was estimated by resorting to the MM/PBSA[37] approach implemented in Amber 14. According to this well validated methodology[25, 27, 28, 38-40], the free energy was calculated for each molecular species(complex, protein, and ligand), and the binding free energy was computed as the difference:

$$\Delta G_{bind} = G_{complex} - (G_{protein} + G_{ligand}) = \Delta H_{bind} - T\Delta S_{bind} = \Delta E_{MM} + \Delta G_{sol} - T\Delta S_{bind}$$

in which ΔH_{bind} is the enthalpic component of ΔG_{bind}(made up of a mechanical energy term ΔE_{MM} and a solvation term ΔG_{sol}) and $T\Delta S_{bind}$ is the conformational entropy upon ligand binding. The per residue binding free energy decomposition was performed exploiting the MD trajectory of each given compound/BVDV RdRp complex, with the aim of identifying the key residues involved in the ligand/protein interaction. This analysis was carried out using the MM/GBSA approach[41, 42], and was based on the samesnapshots used in the binding free energy calculation.

Computational Mutagenesis.

For the computational mutagenesis studies, mutation of the selected residues to alanine was performed on the structure of the wild-type BVDV RdRp protein. Each mutated complex was equilibrated in a 0.15 M NaCl TIP3P water solution to relax eventual conformational perturbations induced by mutation of the residue. Each system was then first subjected to 1000 energy minimization steps, followed by further solvent equilibration for100 ps of MDat 300 K. Finally, the entire system was equilibrated for 2 ns at 300 K. The subsequent MD simulation was conducted with Amber 14 as described above.

Pharmacological section

Expression of the BVDV-NS5BD24 polymerase.

Expression and purification of the BVDV-NS5BΔ24 polymerase were performed as described in details in our previous work[25]. In brief, the expression plasmid encoding the His-tagged C-terminal 24-aminoacid-deleted BVDV-NS5B was introduced into the Escherichia coli strain Rosetta™2(DE3)pLysS (Novagene) by chemical transformation. Transformant bacteria were cultured overnight at 30 °C in 5 mL of lysogeny broth (LB) supplemented with 25 μg/mL kanamycin and 30μg/mL chloramphenicol. Cultures were then diluted into 1 L of LB medium additivated by the same quantities of the two antibiotics, and incubated at 30 C until the A600 reached 0.6–0.7. The culture was then induced overnight with 1 mM isopropyl-β-D-thiogalactopyranoside, after which cells were harvested by centrifugation and stored at 80 °C until purification.

Purification of NS5B proteins.

Cell pellets were thawed and immediately lysed by the addition of 10 mL of CelLytic B (Sigma). Insoluble material was removed by centrifugation at 11,000 rpm for 60 min at 4 C. The soluble extract was applied to a 5-mL column of nickel–nitrilotriacetic acid–agarose (Qiagen), previously equilibrated with the lysis buffer (50 mM NaH2PO4, 300 mM NaCl, 10 mM imidazole, pH 8.0). The column was washed extensively with the wash buffer (50 mM NaH_2PO_4, 300 mM NaCl, 20 mM imidazole, pH 8.0) and the protein was eluted stepwise with the elution buffer containing increasing concentration of imidazole (50 mM NaH_2PO_4, 300 mM NaCl, 50–250 mM imidazole, pH 8.0). The polypeptide composition of each column fraction was monitored via Coomassie-stained SDS–PAGE analysis. Fractions enriched in pure 6xHis-tagged NS5B protein, recovered in the 130–250 mM imidazole eluates, were pooled and dialyzed against a buffer containing 25 mM Tris–HCl, pH7.5, 2.5 mM $MgCl_2$, 1 mM dithiothreitol, and 50% glycerol. Protein concentration was determined by the micro-Bradford method (Bio-Rad) using Bovine Serum Albumin (BSA) as standard. Following dialysis, the purified 6xHis-tagged BVDV-NS5BΔ24 protein was divided into aliquots and stored at -80 °C.

RNA-dependent RNA polymerase assay.

Enzyme assays were performed in 96-well plates using 10 μg/mL poly(rC) (GE Healthcare, formerly Amersham Biosciences) as template, 0.1 μg/mL oligo(rG)12 (Invitrogen) as primer, and80 μM GTP (Invitrogen) as substrate, in a 20 μL reaction mixture containing 20 mM Tris/HCl, pH7.0, 1 mM dithiothreitol, 25 mM NaCl, 20 U/mL RNasin (Promega), 5 mM $MgCl_2$, 5% DMSO, 5%glycerol, and 500 ng of the purified protein. After enzyme/drug pre-incubation for 30 min at room temperature, reactions were started by the addition of GTP. One microliter of

three-fold serial dilutions of test compounds in DMSO 0.5% were added, and the samples were incubated for 120min at 37 C (BVDV-NS5BΔ24). DMSO alone or the nucleotide analog 30-deoxyguanosine-50-triphosphate (30-dGTP) (tebu-bio) were used as negative and positive controls, respectively. Reactions were stopped by adding 2 μL of 200 mM EDTA. 138 microliters of the PicoGreenQuantitation Reagent Molecular Probes diluted 1:345 in TE (Tris/EDTA) buffer were added to each sample, followed by incubation for 5 min at room temperature in the dark. After excitation at 480nm, fluorescence was measured at 520 nm in a fluorescence microplate reader (Infinite F200,Tecan). Effective fluorescence was calculated by subtracting the mean fluorescence of the blank samples and by converting it into % of activity. Percent of residual activity was then plotted *vs.* compound concentrations. Dose–response curves were fit with GraphPad Prism (v. 6.00 for Windows, GraphPad Software, La Jolla California US) to obtain the drug concentration providing 50% inhibition (IC_{50}).

Site-directed mutagenesis.

The plasmid encoding the His-tagged C-terminal 24-aminoacid-deleted BVDV-NS5B was used as the parental clone for all subsequent manipulations. Site-directed mutagenesis was carried out by using a QuickChange mutagenesis kit (Stratagene). The expression of the BVDV NS5B mutants was carried out in the Escherichia coli strain Rosetta™2(DE3)pLysS (Novagene) as described above.

ASSOCIATED CONTENT

Supporting Information.

Results on cytotoxicity and antiviral activity of 3*H*-imidazo[4,5-*g*]quinoline derivatives (**2-5a**, **6-11b**, **12-13c**, **14b**) against other than BVDV ssRNA^{+}, ssRNA^{-}, dsRNA and DNA viruses.

Experimental activity and principal values (PV) of the training test compounds used in the generation of the common feature 3D pharmacophore model.

Dose-response curves from enzyme assays with wild type and selected BVDV RdRp mutants for compounds **D2**, **B1**, **6b**, **E2**, and **F2**.

AUTHOR INFORMATION

Corresponding Author

* Antonio Carta, phone: +39 079228720, e-mail address: acarta@uniss.it

* Sabrina Pricl, phone: +39 040 558 3750, e-mail address: sabrina.pricl@di3.units.it

Author Contributions

▪ These authors equally contributed to this work.

ACKNOWLEDGMENTS

Authors acknowledge the generous financial support from the "Assessorato della Programmazione, Bilancio, Credito e Assetto del territorio, della Regione Autonoma della Sardegna (Italia)", LEGGE REGIONALE 7 AGOSTO 2007.

ABBREVIATIONS

Viral Diarrhea Virus (BVDV), RNA dependent RNA polymerase (RdRp), Dengue Fever (DFV), Yellow Fever (YFV), West Nile (WN), and Japanese Encephalitis (JE), Swine Fever virus (SFV), Border Disease virus (BDV), Human Hepatitis C (HCV), structure-activity relationship

(SAR), electron donating groups (EDGs), electron withdrawing groups (EWGs), selectivity index (S.I.), Hydrogen Bond Acceptor features (HBA), Hydrophobic Aromatic feature (HY_AR), hydrogen bonds (HB), molecular mechanics/Poisson−Boltzmann surface area (MM/PBSA)

REFERENCES

[1] B.D. Lindenbach, C.L. Murray, H.J. Thiel, C.M. Rice, Flaviviridae, in: D.M. Knipe, P.M. Howley (Eds.) Fields Virology., Lippincott Williams & Wilkins, Philadelphia, 2013, pp. 712-746.
[2] T. Kazakov, F. Yang, H.N. Ramanathan, A. Kohlway, M.S. Diamond, B.D. Lindenbach, Hepatitis C virus RNA replication depends on specific cis- and trans-acting activities of viral nonstructural proteins, PLoS pathogens, 11 (2015) e1004817.
[3] T.C. Pierson, M.S. Diamond, Flaviviruses, in: D.M.K.a.P.M. Howley (Ed.), Lippincott Williams & Wilkins., Fields Virology, 2013, pp. 747-794.
[4] J.G. Breugelmans, R.F. Lewis, E. Agbenu, O. Veit, D. Jackson, C. Domingo, M. Bothe, W. Perea, M. Niedrig, B.D. Gessner, S. Yactayo, Y.A. group, Adverse events following yellow fever preventive vaccination campaigns in eight African countries from 2007 to 2010, Vaccine, 31 (2013) 1819-1829.
[5] T.P. Monath, Yellow fever as an endemic/epidemic disease and priorities for vaccination, Bulletin de la Societe de pathologie exotique, 99 (2006) 341-347.
[6] H.J. Thiel, P.G.W. Plagemann, V. Moennig, Pestiviruses, in: D.M.K. B. N. Fields, and P. M. Howley (Ed.) Fields virology, 1996, pp. 1059-1073.
[7] A.M. O'Connor, S.D. Sorden, M.D. Apley, Association between the existence of calves persistently infected with bovine viral diarrhea virus and commingling on pen morbidity in feedlot cattle, American journal of veterinary research, 66 (2005) 2130-2134.
[8] C.C. Chase, G. Elmowalid, A.A. Yousif, The immune response to bovine viral diarrhea virus: a constantly changing picture, The Veterinary clinics of North America. Food animal practice, 20 (2004) 95-114.
[9] B.E. Hessman, R.W. Fulton, D.B. Sjeklocha, T.A. Murphy, J.F. Ridpath, M.E. Payton, Evaluation of economic effects and the health and performance of the general cattle population after exposure to cattle persistently infected with bovine viral diarrhea virus in a starter feedlot, American journal of veterinary research, 70 (2009) 73-85.
[10] V.E. Buckwold, B.E. Beer, R.O. Donis, Bovine viral diarrhea virus as a surrogate model of hepatitis C virus for the evaluation of antiviral agents, Antiviral research, 60 (2003) 1-15.
[11] B.D. Lindenbach, C.M. Rice, Flaviviridae: the viruses and their replication, in: D.M.K.a.P.M. Howley (Ed.) Fields virology, 2001, pp. 991-1041.
[12] P.H. Hayashi, A.M. Di Bisceglie, The progression of hepatitis B- and C-infections to chronic liver disease and hepatocellular carcinoma: epidemiology and pathogenesis, The Medical clinics of North America, 89 (2005) 371-389.

[13] U.J. WHO Hepatitis C Fact sheet N°164, in: http://www.who.int/mediacentre/factsheets/fs164/en/ (Ed.).
[14] A. Baharuddin, A.A. Hassan, G.C. Sheng, S.B. Nasir, S. Othman, R. Yusof, R. Othman, N.A. Rahman, Current approaches in antiviral drug discovery against the Flaviviridae family, Current pharmaceutical design, 20 (2014) 3428-3444.
[15] E. Brochot, F. Helle, C. Francois, S. Castelain, D. Capron, N.K. Eric, G. Duverlie, Which therapeutic option for hepatitis C virus genotype 1?, Scand J Gastroentero, 50 (2015) 470-478.
[16] B.L. Pearlman, C. Ehleben, M. Perrys, The Combination of Simeprevir and Sofosbuvir Is More Effective Than That of Peginterferon, Ribavirin, and Sofosbuvir for Patients With Hepatitis C-Related Child's Class A Cirrhosis, Gastroenterology, 148 (2015) 762-U358.
[17] H. Chai, D. Lim, H. Chai, E. Jung, Molecular Modeling of Small Molecules as BVDV RNA-Dependent RNA Polymerase Allosteric Inhibitors, Bull. Korean Chem. Soc., 34 (2013) 337-350.
[18] G. Vitale, P. Corona, M. Loriga, A. Carta, G. Paglietti, G. Giliberti, G. Sanna, P. Farci, M.E. Marongiu, P. La Colla, 5-acetyl-2-arylbenzimidazoles as antiviral agents. Part 4, European journal of medicinal chemistry, 53 (2012) 83-97.
[19] S. Asthana, S. Shukla, P. Ruggerone, A.V. Vargiu, Molecular mechanism of viral resistance to a potent non-nucleoside inhibitor unveiled by molecular simulations, Biochemistry, 53 (2014) 6941-6953.
[20] S. Asthana, S. Shukla, A.V. Vargiu, M. Ceccarelli, P. Ruggerone, G. Paglietti, M.E. Marongiu, S. Blois, G. Giliberti, P. La Colla, Different molecular mechanisms of inhibition of bovine viral diarrhea virus and hepatitis C virus RNA-dependent RNA polymerases by a novel benzimidazole, Biochemistry, 52 (2013) 3752-3764.
[21] A. Carta, M. Loriga, G. Paglietti, M. Ferrone, M. Fermeglia, S. Pricl, T. Sanna, C. Ibba, P. La Colla, R. Loddo, Design, synthesis, and preliminary in vitro and in silico antiviral activity of [4,7]phenantrolines and 1-oxo-1,4-dihydro-[4,7]phenantrolines against single-stranded positive-sense RNA genome viruses, Bioorganic & medicinal chemistry, 15 (2007) 1914-1927.
[22] M. Wang, K.K. Ng, M.M. Cherney, L. Chan, C.G. Yannopoulos, J. Bedard, N. Morin, N. Nguyen-Ba, M.H. Alaoui-Ismaili, R.C. Bethell, M.N. James, Non-nucleoside analogue inhibitors bind to an allosteric site on HCV NS5B polymerase. Crystal structures and mechanism of inhibition, The Journal of biological chemistry, 278 (2003) 9489-9495.
[23] A. Carta, I. Briguglio, S. Piras, P. Corona, G. Boatto, M. Nieddu, P. Giunchedi, M.E. Marongiu, G. Giliberti, F. Iuliano, S. Blois, C. Ibba, B. Busonera, P. La Colla, Quinoline tricyclic derivatives. Design, synthesis and evaluation of the antiviral activity of three new classes of RNA-dependent RNA polymerase inhibitors, Bioorganic & medicinal chemistry, 19 (2011) 7070-7084.
[24] R. Loddo, I. Briguglio, P. Corona, S. Piras, M. Loriga, G. Paglietti, A. Carta, G. Sanna, G. Giliberti, C. Ibba, P. Farci, P. La Colla, Synthesis and antiviral activity of new phenylimidazopyridines and N-benzylidenequinolinamines derived by molecular simplification of phenylimidazo[4,5-g]quinolines, European journal of medicinal chemistry, 84 (2014) 8-16.
[25] I. Briguglio, R. Loddo, E. Laurini, M. Fermeglia, S. Piras, P. Corona, P. Giunchedi, E. Gavini, G. Sanna, G. Giliberti, C. Ibba, P. Farci, P. La Colla, S. Pricl, A. Carta, Synthesis, cytotoxicity and antiviral evaluation of new series of imidazo[4,5-g]quinoline and pyrido[2,3-g]quinoxalinone derivatives, European journal of medicinal chemistry, 105 (2015) 63-79.

[26] A. Carta, M. Palomba, P. Corona, Synthesis of substituted aminoquinolines as useful intermediates for preparation of aromatic N-tricyclic systems, Heterocycles, 68 (2006) 1715-1722.
[27] G. Giliberti, C. Ibba, E. Marongiu, R. Loddo, M. Tonelli, V. Boido, E. Laurini, P. Posocco, M. Fermeglia, S. Pricl, Synergistic experimental/computational studies on arylazoenamine derivatives that target the bovine viral diarrhea virus RNA-dependent RNA polymerase, Bioorganic & medicinal chemistry, 18 (2010) 6055-6068.
[28] A. Carta, I. Briguglio, S. Piras, G. Boatto, P. La Colla, R. Loddo, M. Tolomeo, S. Grimaudo, A. Di Cristina, R.M. Pipitone, E. Laurini, M.S. Paneni, P. Posocco, M. Fermeglia, S. Pricl, 3-Aryl-2-[1H-benzotriazol-1-yl]acrylonitriles: a novel class of potent tubulin inhibitors, European journal of medicinal chemistry, 46 (2011) 4151-4167.
[29] R.L. Shriner, A. Land, The structure of the bisulfite compound of acetaldehyde, J. Org. Chem., 6 (1941) 888-894.
[30] R. Pauwels, J. Balzarini, M. Baba, R. Snoeck, D. Schols, P. Herdewijn, J. Desmyter, E. De Clercq, Rapid and automated tetrazolium-based colorimetric assay for the detection of anti-HIV compounds, Journal of virological methods, 20 (1988) 309-321.
[31] B.R. Brooks, R.E. Bruccoleri, B.D. Olafson, D.J. States, S. Swaminathan, M.J. Karplus, CHARMM: a program for macromolecular energy, minimization, and dynamics calculations., J. Comput. Chem., 4 (1983) 187-217.
[32] A. Smellie, S.L. Teig, P. Towbin, Poling: promoting conformational variation. , J. Comput. Chem., 16 (1994) 171-187.
[33] Discovery Studio v.2.5, Accerlys, San Diego, CA, USA.
[34] G.M. Morris, R. Huey, W. Lindstrom, M.F. Sanner, R.K. Belew, D.S. Goodsell, A.J. Olson, AutoDock4 and AutoDockTools4: automated docking with selective receptor flexibility., J. Comput. Chem., 30 (2009) 2785−2791.
[35] D.A. Case, J.T. Berryman, R.M. Betz, D.S. Cerutti, T.E.I. Cheatham, T.A. Darden, R.E. Duke, T.J. Giese, H. Gohlke, A.W. Goetz, N. Homeyer, S. Izadi, P. Janowski, J. Kaus, A. Kovalenko, T.S. Lee, S. LeGrand, P. Li, T. Luchko, R. Luo, B. Madej, K.M. Merz, G. Monard, P. Needham, H. Nguyen, H.T. Nguyen, I. Omelyan, A. Onufriev, D.R. Roe, A. Roitberg, R. Salomon-Ferrer, C.L. Simmerling, W. Smith, J. Swails, R.C. Walker, J. Wang, R.M. Wolf, X. Wu, AMBER 2015, in: D.M. York and P.A. Kollman, University of California, San Francisco, 2015.
[36] W.L. Jorgensen, J. Chandrasekhar, J.D. Madura, R.W. Impey, M.L. Klein, Comparison of simple potential functions for simulating liquid water., J. Chem. Phys., 79 (1983) 926-935.
[37] I. Massova, P.A. Kollman, Combined molecular mechanical and continuum solvent approach (MM-PBSA/GBSA) to predict ligand binding., Perspectives in Drug Discovery and Design., 18 (2000) 113-135.
[38] E. Laurini, D. Marson, V. Dal Col, M. Fermeglia, M.G. Mamolo, D. Zampieri, L. Vio, S. Pricl, Another brick in the wall. Validation of the sigma1 receptor 3D model by computer-assisted design, synthesis, and activity of new sigma1 ligands, Molecular pharmaceutics, 9 (2012) 3107-3126.
[39] S. Brune, D. Schepmann, K.H. Klempnauer, D. Marson, V. Dal Col, E. Laurini, M. Fermeglia, B. Wunsch, S. Pricl, The sigma enigma: in vitro/in silico site-directed mutagenesis studies unveil sigma1 receptor ligand binding, Biochemistry, 53 (2014) 2993-3003.
[40] L. Brambilla, D. Genini, E. Laurini, J. Merulla, L. Perez, M. Fermeglia, G.M. Carbone, S. Pricl, C.V. Catapano, Hitting the right spot: Mechanism of action of OPB-31121 a novel and

potent inhibitor of the Signal Transducer and Activator of Transcription 3 (STAT3). Molecular oncology, 9 (2015) 1194-1206.
[41] V. Tsui, D.A. Case, Theory and applications of the generalized Born solvation model in macromolecular simulations, Biopolymers, 56 (2000) 275-291.
[42] A. Onufriev, D. Bashford, D.A. Case, Modification of the generalized born model suitable for macromolecules. , J. Phys. Chem. B, 104 (2000) 3712-3720.

Highlights

In this work, we present linear N-polycyclic systems that inhibits BVDV infection.

All derivates have been investigated for their anti-BVDV activity.

Several compounds showed micromolar activity against BVDV.

In silico/*in vitro* analysis offer a molecular rationale for the BVDV RdRp NS5B affinity.

Compound 6b emerged as a potent inhibitor of this *Pestivirus*.